Novel Platelet Substitutes: Disk-Shaped Biodegradable Nanosheets and their Enhanced Effects on Platelet Aggregation

Yosuke Okamura,[†] Yoshihito Fukui,[†] Koki Kabata,[†] Hidenori Suzuki,[‡] Makoto Handa,[§] Yasuo Ikeda,[†] and Shinji Takeoka*,[†]

Department of Life Science and Medical Bioscience, Graduate School of Advanced Science and Engineering, Waseda University, TWIns, Tokyo, 162-8480, Japan, Center for Electron Microscopy, Tokyo Metropolitan Institute of Medical Science, Tokyo, 113-8613, Japan, and Department of Transfusion Medicine and Cell Therapy, Keio University, Tokyo, 160-8582, Japan.
Received July 23, 2009

We have studied biocompatible spherical carriers carrying a dodecapeptide, HHLGGAKQAGDV (H12), on their surface as platelet substitutes. This peptide is a fibrinogen γ-chain carboxy-terminal sequence (γ400−411) and specifically recognizes the active form of glycoprotein IIb/IIIa on activated platelets. Our purpose is to assess the possibility of making a novel platelet substitute consisting of disk-shaped nanosheets having a large contact area for the targeting site, rather than conventional small contact area spherical carriers. The H12 peptide was conjugated to the surface of the free-standing nanosheets made of biodegradable poly(D,L-lactide-*co*-glycolide) (PLGA). These H12-PLGA nanosheets were fabricated onto 3 μm disk-shaped patterned hydrophobic octadecyl regions on a SiO_2 substrate. By way of comparison, spherical H12-PLGA microparticles with the same surface area and conjugation number of H12 were also prepared. The resulting H12-PLGA nanosheets specifically interacted with the activated platelets adhered on the collagen surface at twice the rate of the H12-PLGA microparticles under flow conditions, and showed platelet thrombus formation in a two-dimensional spreading manner. Thus, H12-PLGA nanosheets might be a suitable candidate novel platelet alternative substitute for infused human platelet concentrates for the treatment of bleeding in patients with severe thrombocytopenia.

INTRODUCTION

Transfusion of platelet concentrates by blood donation is currently the only means of efficiently treating or preventing bleeding caused by quantitative platelet disorders. Particularly, the supply of platelet concentrates is always in a critical situation because of the short shelf life (4 days in Japan, 5−7 days in the United States and Europe) under stringent storage conditions. Moreover, the risk of blood-borne infections such as bacterial sepsis and acute immune reactions remains a major concern for allogeneic platelet transfusion (*1, 2*). For these reasons, a number of trials have been conducted to develop platelet substitutes (artificial platelets) reproducing platelet functions such as infusible platelet membranes (IPMs) (*3*), fibrinogen-bonded red blood cells (*4*), fibrinogen-bearing liposomes (*5*), fibrinogen-coated albumin microcapsules (Synthocyte) (*6*), and arginine-glycine-asparaginic acid (RGD) peptide-bound red blood cells (Thromboerythrocytes) (*7*). All platelet substitutes proposed so far consist of materials derived from blood components and are micrometer sized.

Glycoprotein (GP) IIb/IIIa exists on the membrane of distinctive disk-shaped platelets at the dimensions of 2.5−3.0 by 0.2−0.5 μm and changes its shape from inactive to active when platelets adhere to collagen exposed on the sites of vascular injury (*8, 9*). The activated GPIIb/IIIa acts as a receptor for bifunctional fibrinogen, which leads to platelet aggregation. Several sequences in fibrinogen have been designated as GPIIb/IIIa recognition sites: the RGD-based sequences ^{95}RGDF^{98} and ^{572}RGDS^{575} in the Aα chains and ^{400}HHLGGAKQAGDV^{411} (H12, the fibrinogen γ-chain dodecapeptide) in the carboxyl-terminal of the γ-chain (*10, 11*). We selected H12 for this study from general observations that H12 interacts with GPIIb/IIIa specifically, whereas RGD-related peptides are promiscuous for many integrins from various cell types (*12*).

Our strategy for the development of platelet substitutes has been straightforward: biocompatible spherical carriers such as phospholipid vesicles (liposomes) (*13−15*) and polymerized albumin particles (*16, 17*) are specifically accumulated at sites of vascular injury, and fill up the injury sites by virtue of their own mass. In order to construct carriers having a specific accumulation ability for the activated GPIIb/IIIa on the platelet, we conjugated an H12 sequence to these carriers and succeeded in the preparation of H12-conjugates, which dose-dependently reduced the bleeding time in rats or rabbits with thrombocytopenia *in vivo* (*14, 15, 18−20*).

Sheet-shaped carriers, having a large contact area for a targeting site, would have an ultimate advantage over spherical carriers, which have an extremely small contact area. Recently, several approaches have been implemented for fabrication of free-standing nanosheets (often called nanofilms and nanomembranes), including the use of polymers and/or inorganic materials such as cast films (*21*), layer-by-layer films of polyelectolytes (*22−24*), cross-linked amphiphilic Langmuir−Blodgett films (*25*), and self-assembled monolayers (SAMs) (*26*). They have been developed as applications in a variety of fields such as nanoseparation membranes, nanosensors, and functional nanofilms for electrochemical and photochemical applications. However, there have been no reports on the fabrication of free-standing nanosheets with suitable biocompatibility and biodegradability for biomedical application.

Organosilane SAMs have been widely used in applications designed to change the physical and chemical properties of the surfaces of glass, quartz, and SiO_2/Si wafers (*27*). It is generally

* To whom correspondence should be addressed. E-mail: takeoka@waseda.jp, Tel: +813-5369-7324, Fax: +813-5369-7324.
[†] Waseda University.
[‡] Tokyo Metropolitan Institute of Medical Science.
[§] Keio University.

10.1021/bc900325w CCC: $40.75
Published on Web 09/29/2009

easy to construct patterned SAMs with uniform size and shape on SiO_2 using conventional photolithography processes (*28*). They are excellent tools for immobilization of proteins (redox proteins (*29*) and enzymes (*30*)) via covalent or noncovalent bonding with various terminal groups of the SAMs, and for two-dimensional close-packed particle array via a micromold method and lateral capillary force (*31*). Recently, we proposed a novel method for the preparation of free-standing 100 nm thick, uniformly shaped microsized nanosheets derived from polystylene nanoparticles using patterned hydrophobic SAMs on the SiO_2 substrate (*32*).

Our main purpose here was to assess the possibility of constructing disk-shaped nanosheets as a novel platelet substitute. In this study, H12 was conjugated to the surface of free-standing biodegradable poly(D,L-lactide-*co*-glycolide) (PLGA) platelet-like nanosheets (H12-PLGA nanosheets), which had been attached to a SiO_2 substrate patterned with 3 μm disk-shaped hydrophobic regions of octadecyltrimethoxysilane-SAM (ODS-SAM). Furthermore, we explore the enhanced effects on platelet thrombus formation of the H12-PLGA nanosheets in comparison with that of the H12-PLGA microparticles under flow conditions.

MATERIALS AND METHODS

Reagents. P-type Si (100) wafers (below 0.02 Ω cm) covered with thermally grown silicon oxide (approximately 200 nm) were purchased from KST World Co. (Fukui, Japan). *n*-Octadecyltrimethoxysilane (ODS, 97%) and 2-methyl[(polyethyleneoxy)propyl] trichlorosilane (Cl_3Si-mPEO, M_w: 422−558, >97%) were purchased from Gelest Inc. (Morrisville, PA). Poly(D,L-lactide-*co*-glycolide) (PLGA) (lactide/glycolide = 85:15, M_w 20 kDa) was purchased from Polysciences Inc. (Warrington, PA). Chitosan (M_w 88 kDa) and poly(vinyl alcohol) (PVA, M_w 22 kDa (99% hydrolyzed), 20 kDa (87−89% hydrolyzed)) were obtained from Nacalai Tesque, Inc. (Kyoto, Japan) and Sigma-Aldrich Co. (Saint Louis, MO), respectively. Poly(ethylene glycol), α-(3-[3-maleimido-1-oxopropyl]amino) propyl-ω-succinimidyl carboxypentyloxy poly(ethylene glycol) (MALPEG-NHS, M_w 5.0 kDa) was purchased from NOF Co. (Tokyo, Japan). Fibrinogen γ-chain dodecapeptide (C-HHLGGAKQAGDV, Cys-H12) was synthesized with a solid-phase synthesizer by BEX Co. (Tokyo). The platelet fluorescent dye 3,3′-dihexyloxacarbocyanine iodide ($DiOC_6$) and dioctadecyloxacarbocyanine perchlorate ($DiOC_{18}$), a fluorescent dye for PLGA particles, were purchased from Invitrogen Co. (Eugene, OR). Fluorescamine was purchased from Sigma-Aldrich Co.

SAM Preparation. Silicon wafers (size 3 cm × 3 cm) were treated with a piranha solution (96% H_2SO_4/30% H_2O_2 = 4:1 (v/v)) at 120 °C followed by rinsing with distilled water. The resulting wafers were placed in a 100 mL Teflon vial containing a glass cup filled with 200 μL ODS liquid. The vials were sealed with a cap and then heated for 8 h at a constant temperature of 110 °C in a glovebox to prepare a hydrophobic ODS-SAM on the silicon oxide (*33*).

Patterning Processes. The ODS/mPEO-SAM patterned with hydrophobic octadecyl regions and hydrophilic poly(ethylene oxide) regions on the substrate was prepared by conventional photolithography and chemical conjugation processes. The ODS-SAM on the silicon oxide (size 3 cm × 3 cm) was covered with photoresist (OFPR-800 500 cP, Tokyo Ohka Kogyo, Co. Ltd., Kanagawa, Japan), and was irradiated with a UV lamp (350 nm, MA-10, Mikasa Ltd., Tokyo) using a photomask (size 5 cm × 5 cm, patterning 3 μm disk, Topic Co., Ltd., Saitama, Japan). After developing (NMD-3), the substrate was exposed to an oxygen plasma (Plasma Reactor PR301, Yamato Scientific Co. Ltd., Tokyo) at an input power of 200 W and an oxygen flow rate of 80 sccm for removal of the ODS. The photoresist was removed by acetone washing, and then the patterned ODS-SAM substrate was immersed in a 2 mM solution of Cl_3Si-mPEO in toluene at r.t. for 24 h in a glovebox in order to reduce the nonspecific adsorption of the PLGA nanoparticles, as suggested in an original report by Cecchet et al. (*34*).

Preparation of PLGA Nano- and Microparticles. PLGA nanoparticles were prepared by a very successful emulsion diffusion−evaporation technique, as reported previously (*35*). The methodology in brief is described as follows. First, 200 mg of PLGA was dissolved in 10 mL ethyl acetate at r.t. The organic phase was then added to an aqueous solution (10 mL) containing 200 mg PVA (87−89% hydrolyzed) as a stabilizer and 30 mg chitosan with stirring. The emulsion was stirred at r.t. for 3 h before homogenizing at 30 000 rpm for 10−70 min (Physcotron NS-51, Microtec, Co. Ltd., Chiba, Japan). Distilled water (50 mL) was gradually added to the emulsion with stirring, and then stirring was continued in a water bath maintained at 40 °C to remove the organic solvent. The uncoated polymer reagents such as PVA and chitosan were removed by repeated centrifugation (35 000*g*, 10 min, 4 °C) and washing with phosphate buffer (PB, pH 7.4) to obtain the purified PLGA nanoparticles. The particle diameter was analyzed by a dynamic light-scattering (DLS) method (N4 PLUS; Beckman-Coulter, Fullerton, FL).

In addition, PLGA microparticles were prepared by the same technique. Two hundred milligrams of PLGA was dissolved in 10 mL methylene chloride at r.t. The organic phase was then added to an aqueous solution (10 mL) containing 200 mg PVA (87−89% hydrolyzed) and 30 mg chitosan at r.t. under 1000 rpm stirring without homogenization. Distilled water (50 mL) was gradually added to the emulsion under stirring, and then stirred at 40 °C to remove the organic solvent. The uncoated polymer reagents such as PVA and chitosan were removed by repeated centrifugation (2200*g*, 5 min, 4 °C) and washing with PB (pH 7.4) to obtain the purified PLGA microparticles.

The particle concentration was calculated from the volume ratio of the PLGA particles in the suspension as follows: the suspension was mixed with a PEG solution (M_w = 100 kDa, final concentration 25 mg/mL), inserted into a hematocrit capillary tube, and then precipitated by centrifugation (15 000*g*, 10 min, r.t.) to measure the volume ratio of PLGA particles. The particle concentration (N, particles/mL) was calculated by eq 1:

$$N = 3B/(A - B) \times 4\pi r^3 \times 10^3 \quad (1)$$

where $A(m)$, $B(m)$, and $r(m)$ were the height of the suspension surface from the bottom of the capillary tube, the height of the particle precipitate, and the particle radius, respectively.

The amino groups in the surface of the PLGA nano- and microparticles, which were derived from chitosan, were calculated from the fluorescent intensity after a fluorescamine reaction as follows: fluorescamine in acetone (0.1 M, 10 μL) was added to the PLGA particle suspension in a boracic acid buffer (pH 8.0) at a concentration of 2.0×10^{11} /mL. The same experiment was performed for the control PLGA particles (not modified with chitosan). The fluorescent intensities after incubation at r.t. for 10 min were measured (E_x = 390 nm, E_m = 475 nm) with a spectrofluorometer (FP-750, JASCO, Tokyo), and the amino groups par PLGA particle were calculated from the difference in intensities between particles before and after chitosan modification and the extrapolation of calibration was performed using a glycine solution of which concentration was varied from 0.1 to 2 μM.

The glass transition temperature (T_g) of the PLGA particles was measured by differential scanning calorimetry (DSC, Thermo plus DSC 8230, Rigaku Co., Osaka, Japan). The analysis was performed with an approximately 10 mg freeze−dried

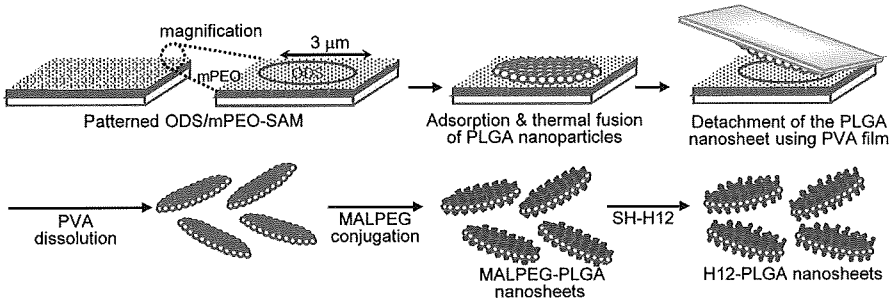

Figure 1. Preparative scheme of free-standing PLGA nanosheets carrying H12 using a patterned ODS/mPEO-SAM on a SiO_2 substrate.

sample under a dynamic nitrogen atmosphere at a heating rate of 10 °C/min.

Preparation of the Free-Standing PLGA Nanosheets Carrying H12. As shown in Figure 1, the substrate having the patterned ODS/mPEO-SAM on the surface was immersed into a PB suspension (pH 7.0) of the PLGA nanoparticles at a concentration of 1.0×10^{12} /mL. After withdrawing the substrate from the suspension, the suspension remaining on the substrate was slowly blown off with a horizontal N_2 flow in order to adsorb the PLGA nanoparticles onto the hydrophobic octadecyl patterned region, and then the substrate was immediately washed with distilled water. The operations of adsorption and washing of PLGA nanoparticles on the substrate was repeated ten times to obtain a closely packed pattern of PLGA nanoparticles. After drying the substrate under N_2 flow, it was heated at 70 °C for 2 min to initiate thermal fusion of the adsorbed PLGA nanoparticles. A PVA solution (50 mg/mL, 0.5 mL) was cast on the substrate and dried at r.t. for 15 h to make a supporting film. After peeling off the resulting PVA film, it was dissolved in a PB solution at pH 7.0, and PVA was removed by centrifugation (8000*g*, 5 min, 4 °C) to obtain a suspension of free-standing PLGA nanosheets. A solution of MALPEG in DMSO (1 mM, 100 μL) was added to the suspension and incubated at r.t. for 20 min. The unreacted MALPEG was removed by centrifugation (8000*g*, 5 min, 4 °C). Finally, the nanosheet suspension was reacted with H12 in PB (1 mM, 70 μL) at r.t. for 12 h, and the unreacted reagents were removed by repeated centrifugation (8000*g*, 5 min, 4 °C) to obtain the purified (MALPEG)PLGA nanosheets carrying H12 (H12-PLGA nanosheets).

The densities of MALPEG and H12 conjugated to the surface of the PLGA nanosheet were determined by quantifying each unreacted reagent in the supernatant of the nanosheets using high-pressure liquid chromatography (HPLC) on a TSK-GEL G3000PW_{XL} column (7.8 mm o.d. × 300 mm h using a mobile phase of 36% acetonitrile and 0.1% trifluoroacetic acid at 1 mL/min). The unreacted reagents were detected using a refractive index (RI) detector and the absorbance at 220 nm.

The concentration of PLGA nanosheets was calculated as follows. First, $DiOC_{18}$ (1 mM, 300 μL) in DMSO was added to the solution of PLGA in ethyl acetate before addition to an aqueous stabilizer as described above. After preparation of the free-standing PLGA nanosheets using $DiOC_{18}$-labeled PLGA nanoparticles, the nanosheets were dissolved in DMSO and the fluorescent intensity was measured (E_x = 485 nm, E_m = 500 nm, ARVO SX, LKB-Wallac, Bromma, Sweden). The PLGA nanosheet concentration was calculated from an extrapolation of the calibration curve of the $DiOC_{18}$-labeled PLGA nanoparticles at a concentration of 1.2×10^9 to 1.5×10^{11} /mL, assuming that the PLGA nanoparticles were arranged and closely packed as a monolayer.

The resulting nanosheets were observed with a Hitachi S-4500 field emission scanning electron microscope (SEM) as follows: the nanosheets adsorbed on a silicon substrate and the free-standing nanosheets collected on glass plate (diameter 24 mm, thickness 0.12−0.17 mm) coated with a poly(L-lysine) were coated with osmium tetroxide (thickness: ca. 20 nm) using an osmium plasma coater (NL-OPC80, Nippon Laser & Electronics Lab., Nagoya, Japan), and were observed with an SEM at an accelerating voltage of 10 kV.

Interaction of Platelets or H12-PLGA Nanosheets with the Collagen Surface Using Imitation Thrombocytopenia Blood under Flow Conditions. Imitation thrombocytopenia blood was prepared as follows. Whole blood treated with a thrombin inhibitor, D-Phe-Pro-Arg-chloromethylketone (PPACK, 40 μM), was filtered with a leukocyte removal filter (NEO1J, Nihon Poll Co., Ltd., Tokyo), which removed platelets as well as leukocytes. The residual platelet count of the filtered blood was determined to be $(6.0 \pm 2.0) \times 10^3$ /μL, and the final platelet count was adjusted to 2.0×10^4 /μL by PRP addition. This blood preparation was termed imitation thrombocytopenia blood.

Collagen I-A (3.0 mg/mL) was suspended in PBS at 4 °C (30 μg/mL), and a glass plate (diameter 24 mm, thickness 0.5 mm) was immersed into the collagen suspension at 4 °C for 8 h. The glass plate was carefully rinsed with PBS and immersed in a bovine serum albumin solution (20 mg/mL) at r.t. for 2 h before a perfusion study was performed as described below.

In the perfusion study, either platelets or H12-PLGA nanosheets were labeled with a fluorescent marker (platelets, $DiOC_6$; nanosheets, $DiOC_{18}$). The imitation thrombocytopenia blood (2.0×10^4/μL) in the absence or presence of the H12-PLGA nanosheets (2.0×10^5/μL) were placed in a recirculating flow chamber mounted on an epifluorescent microscope (ECLIPS TE300, Nikon, Tokyo) equipped with a CCD camera, and the interaction of the nanosheets with the collagen immobilized on the surface was observed. All perfusion studies were performed at 37 °C. Calculation of the surface coverage of platelets or the H12-PLGA nanosheets on the plates was carried out with an image processor, Argus-20 (Hamamatsu Photonics, Hamamatsu, Japan). The interaction of nanosheets with platelets was observed with an SEM as described above.

RESULTS AND DISCUSSION

Fabrication of the Free-Standing H12-PLGA Nanosheets. Fabrication of the free-standing PLGA nanosheets carrying H12 involved several sets of procedures. This section summarizes the results at each stage. The nanosheets themselves were prepared starting from unimodal PLGA nanoparticles prepared, as described above, by a combination of emulsion−diffusion−evaporation and homogenization, following the original report of Ravi-Kumar et al. (*35*). We used a blend of PVA and chitosan as a stabilizer for the PLGA nanoparticles. A recent paper indicates that PVA will remain on the surface of the nanoparticles despite repeated washing of the stabilizer because PVA forms an interconnected network with the polymer at the interface (*36*). Chitosan on the surface of the nanoparticles is

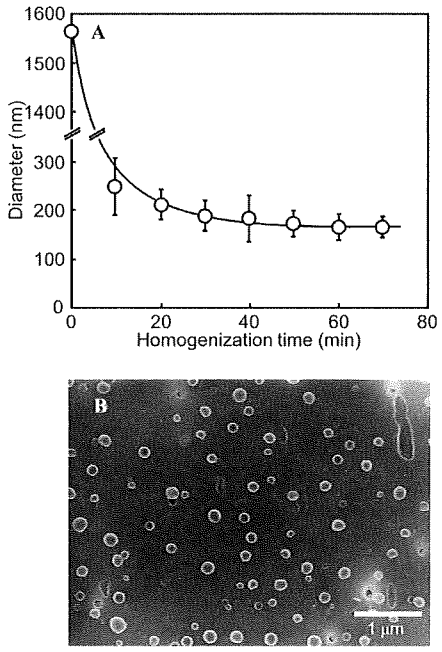

Figure 2. PLGA nanoparticles prepared by a combination of emulsion–diffusion–evaporation plus homogenization techniques. (A) Control of the diameter of the PLGA nanoparticles by the homogenization time. (B) SEM image of the resulting nanoparticles after homogenization for 60 min collected on a membrane filter (pore size: 0.05 μm).

used to conjugate various molecules to its amino groups. The concentration of the stabilizers (PVA and chitosan) has also been optimized for the smallest particle size (*35*). According to the optimum procedure, the emulsion of PLGA in the PVA–chitosan solution was stirred for 3 h at r.t. to produce particles with a diameter of 1563 ± 768 nm (Figure 2A). When the emulsion was homogenized at 30 000 rpm, the diameter decreased with increasing homogenization time and plateaued at 164 ± 26 nm at 60 min after homogenization (Figure 2A). We also confirmed that the diameter of the resulting PLGA nanoparticles was approximately 160 nm by SEM observation (Figure 2B). The amount of the amino groups introduced on the surface of the PLGA nanoparticle was quantified to be approximately 3.8×10^3 molecules, indicating that the surface of the PLGA nanoparticles was fully coated with chitosan to be conjugated H12 molecules.

Using the PLGA nanoparticles, we prepared free-standing PLGA nanosheets carrying H12 by a combination of the four processes shown in Figure 1:

1. Specific adsorption of the PLGA nanoparticles onto the disk-patterned hydrophobic ODS regions of ODS/mPEO-SAM.
2. Fabrication of PLGA nanosheets via thermal fusion of the adsorbed nanoparticles.
3. Preparation of the free-standing nanosheets by detachment from the disk-patterns using a water-soluble PVA as a sacrificial supporting film.
4. Conjugation of H12 to the surface of the nanosheets.

In the first step, a conventional dry patterning process was adopted for the specific adsorption of the PLGA nanoparticles onto the disk-patterned ODS/mPEO-SAM. When the dispersion of the nanoparticles was dropped on the substrate and the dispersion remaining on the substrate was then slowly blown off with a horizontal stream of N_2 gas, the nanoparticles were arranged as a monolayer on the entire substrate, regardless of hydrophobic or hydrophilic regions (data not shown). It is possible that assembly of the PLGA nanoparticles leads to nucleation initiated by capillary forces and growth driven by a laminar flow to evaporate water, thereby forcing the particles to arrange in a monolayer (*37*). The following immediate and repeated washings of the substrate with PB (pH 7.0) detached the PLGA nanoparticles from the hydrophilic mPEO region, leaving nanoparticles firmly adsorbed on the hydrophobic disk patterns of ODS (3 μm) via a hydrophobic interaction. In fact, the net charge of the PLGA nanoparticles at pH 7.0 was nearly zero from the ζ-potential analysis. After repeating the adsorption of the PLGA nanoparticles and washing cycle ten times, the PLGA nanoparticles were closely packed in a monolayer pattern, as shown in Figure 3A,B.

Furthermore, the substrate could be reused at least ten times by sonication in acetone and distilled water (Supporting Information Figure S1). In the case of substrates having bare SiO_2 regions (not modified with mPEO), the nanoparticles were nonspecifically adsorbed to the SiO_2 region as well as the ODS region, and the substrate could not be reused even after heavy sonication (Supporting Information Figure S2A). Using PLGA nanoparticles at 1/10th of the usual concentration (1.0×10^{11}/mL) could prevent the nonspecific adsorption. However, repeated adsorption plus washing over 60 times were required for closely packing of the PLGA nanoparticles in this case (Supporting Information Figure S2B). These results indicated that mPEO modification to the SiO_2 region contributes not only to the inhibition of nonspecific adsorption of the nanoparticles, but also to drastic shortens the preparation time.

Next, the T_g of freeze–dried PLGA nanoparticles was found to be 58.8 °C by a DSC measurement in order to set the temperature required for thermal fusion of the nanoparticles adsorbed on the disk patterns. When the nanoparticle-covered substrate was heated at 60 °C for 2 min with a hotplate, the neighboring PLGA nanoparticles were sufficiently fused to form nanosheets. Heating at 60 °C for 1 min or less was insufficient to properly fuse the particles into nanosheets. On the other hand, heating over 5 min resulted in melting and spreading of the PLGA outward from the disk patterns.

In the second step, the transference of the nanosheets to a supporting PVA film is a convenient method to obtain an aqueous dispersion of the nanosheets (*32*). In practice, the PVA solution was cast on the patterned substrate on which the nanosheets had been fabricated, and dried at r.t. for 15 h. The PVA film peeled off from the substrate was tough and transparent as shown in Figure 3C. SEM observation of the PVA film confirmed that the PLGA nanosheets were completely transferred to the PVA film, and no nanosheets were remained on the substrate (data not shown). Such complete transfer is possible because the hydrogen bonding between the PVA film and the PLGA nanosheets is stronger than the van der Waals interaction of the dried nanosheets with the CH_3-terminal ODS. These results are in agreement with the report by Stroock et al. (*38*), describing the exquisite transfer of an LbL film prepared on hydrophobic SAM patterns to a poly(acrylic acid) (PAA) film. They obtained a suspension by dispersing the PAA film in an aqueous solution. We also used this latter technique for our nanosheets, using PVA as a supporting film. In this case, we could obtain free-standing PLGA nanosheets by dissolution of the PVA film, which is readily soluble in PB at pH 7.4. The nanosheets were collected on a glass plate coated with poly(L-lysine). Thanks to efficient adsorption as a result of the electrostatic interaction, abundant nanosheets with a disk-shaped structure were observed on the plate by SEM, as shown in Figure 3D. This result confirmed that the neighboring PLGA nanoparticles had fused effectively and were sufficiently connected to retain a two-dimensional shape. Fluorescence measurements gave an estimate of approximately 1.2×10^7 nanosheets/mL for the concentration of the resulting disk-shaped nanosheets.

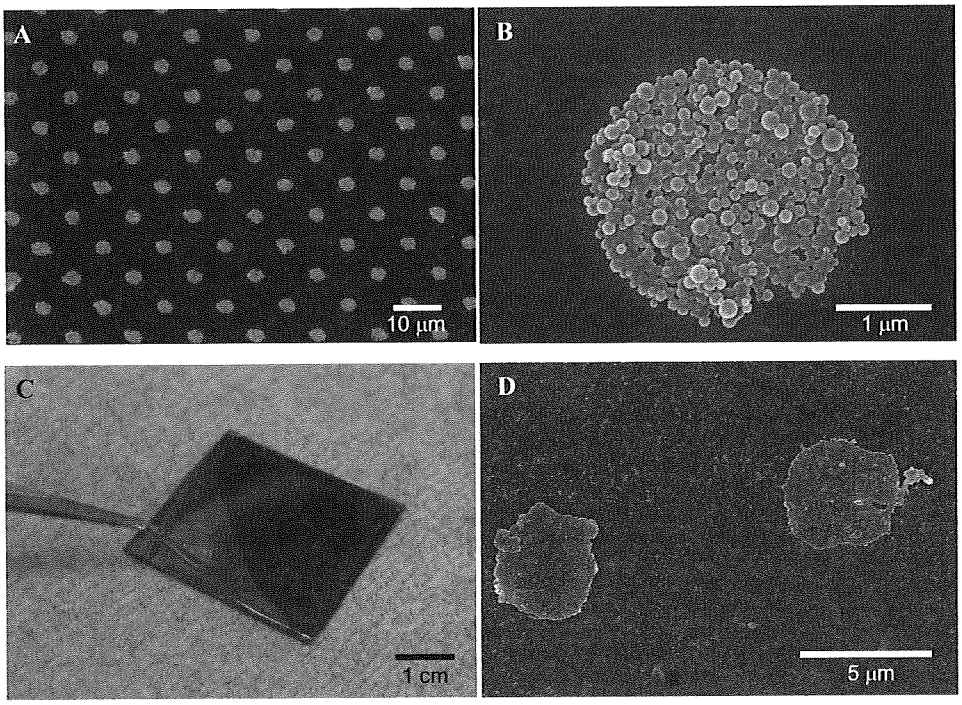

Figure 3. (A) SEM image of the PLGA nanoparticles adsorbed specifically onto the disk-patterned ODS/mPEO-SAM. (B) Magnified SEM image of (A). (C) Photo of the PLGA nanosheets transferred from the ODS/mPEO-SAM to the PVA film. (D) SEM image of the free-standing PLGA nanosheets after dissolution of the resulting PVA film.

In the final step, H12 molecules were conjugated to the surface of the PLGA nanosheets via the maleimide group of MALPEG-NHS as a cross-linker, which targeted the amino groups derived from chitosan. The number of H12 molecules on one nanosheet was indirectly estimated to be approximately 6.1×10^5 molecules from the quantification of free H12 molecules. For an average surface area per nanosheet of 14.9 μm^2, the resulting conjugation density on the nanosheet surface was approximately 4.1×10^4 molecules/μm^2. The density seems to be sufficient for our purposes for the following reasons: In our previous studies on H12-nanoparticles (liposomes and albumin nanoparticles), a conjugation density of H12 over 4.0×10^4 molecules/μm^2 was necessary to maintain the binding ability toward activated platelets, based on flow cytometric analyses and the hemostatic evaluation of the nanoparticles using thrombocytopenic rats *in vivo* (*18*−*20*).

Fabrication of H12-PLGA Microparticles. In order to reveal the differences in hemostatic abilities of disk-shaped and spherical carriers, we also tried to fabricate H12-PLGA microparticles having the same surface area and conjugation number of H12 as those of disk-shaped nanosheets. Using conventional emulsion−diffusion−evaporation methodology with PVA/chitosan as a stabilizer, we obtained PLGA microparticles with an average diameter of 2.2 ± 0.5 μm, corresponding to a surface area per microparticle (15.2 μm^2) that is almost the same as that of the nanosheet. After H12 molecules were bonded to the surface of the particles via MALPEG-NHS, the number of H12 molecules on one microparticle were indirectly estimated to be approximately 6.5×10^5 molecules, corresponding to a conjugation density of approximately 4.2×10^4 molecules/μm^2, a value very close to that of H12-PLGA nanosheets.

Enhanced Effects of H12-PLGA Nanosheets on Platelet Aggregation under Flow Conditions. In order to explore whether the H12-PLGA nanosheets have a specific binding ability toward activated platelets under flow conditions, we prepared imitation thrombocytopenia blood, adjusting the platelet count to 2.0×10^4 /μL (corresponding to one-tenth of that of normal blood). In comparison, we also performed the same experiment using the H12-PLGA microparticles having the same surface area and H12 conjugation number as the nanosheets. When the blood containing the H12-PLGA nanosheets or H12-PLGA microparticles, which were labeled with the fluorescent marker $DiOC_{18}$, was allowed to flow over the collagen surface at a shear rate of 150 s^{-1}, both carriers gradually adhered and accumulated significantly on the surface in a time-dependent manner (Supporting Information movie S1). It was interesting to note that the H12-PLGA nanosheets adhered on the surface at twice the rate of the H12-PLGA microparticles; the adhesive rates of the H12-PLGA nanosheets and H12-PLGA microparticles were calculated to be 14.5 ± 2.3 and 7.7 ± 1.3 /mm²/s, respectively (Figure 4). A simulation by Mortensen et al. suggests that ellipsoidal particles tend to align in the near-wall region of the turbulent shear flow, and that their alignment increases with an increase in the particle aspect ratio between the semiminor and semimajor axis of ellipsoid from 10 to 50

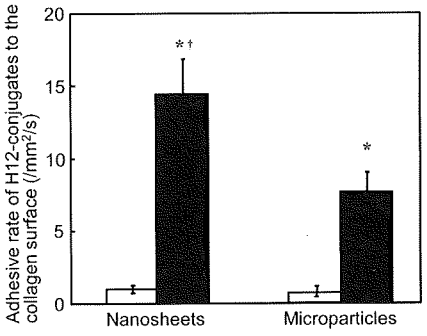

Figure 4. Adhesive rates of the H12-PLGA nanosheets and H12-PLGA microparticles in the thrombocytopenic blood toward the collagen-immobilized surface at a shear rate of 150 s^{-1}. Solid or open columns show H12-conjugates or nonconjugates, respectively. Count of platelets and the H12-PLGA nanosheets or H12-PLGA microparticles was $2.0 \times 10^4/\mu L$. $^*P < 0.05$ for H12-PLGA nanosheets or H12-PLGA microparticles group vs PBS group, and $^\dagger P < 0.05$ for H12-PLGA nanosheets group vs H12-PLGA microparticles group. Data are expressed as the mean ± SD of three independent experiments.

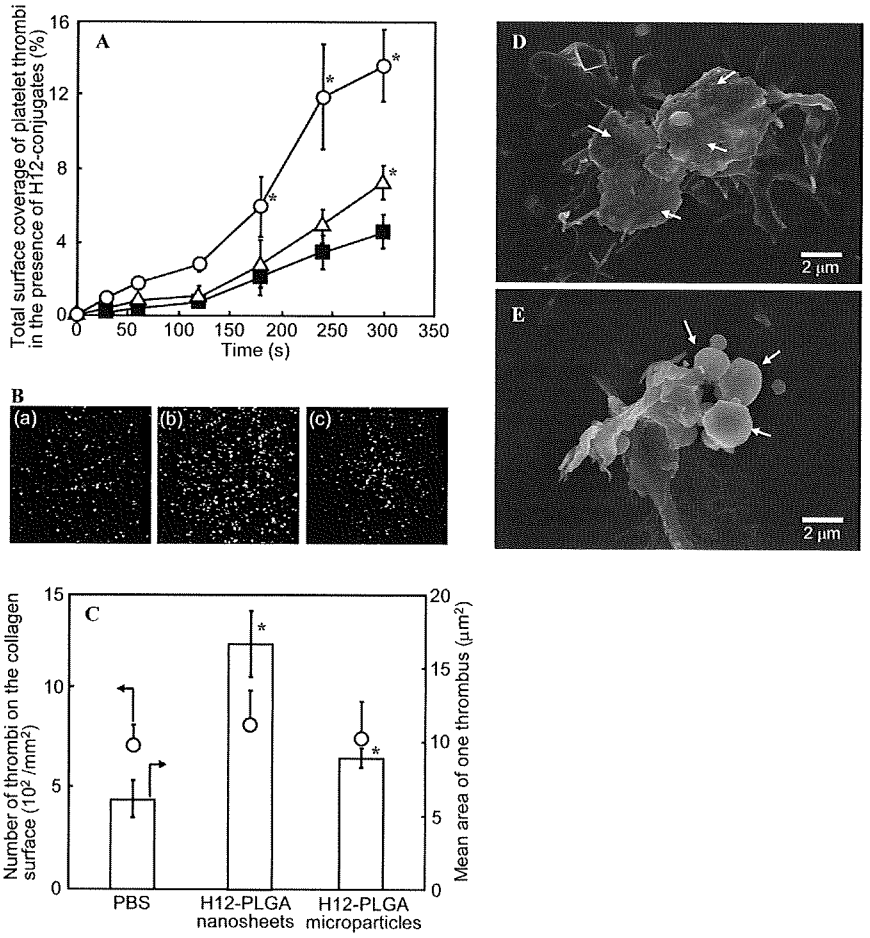

Figure 5. Enhancement of platelet aggregation by H12-PLGA nanosheets under flow conditions. Data are expressed as the mean ± SD of three independent experiments. (A) Time course of the surface coverage of platelet thrombi in the imitation thrombocytopenia blood on the collagen surface after addition of (○) H12-PLGA nanosheets, (△) H12-PLGA microparticles, and (■) PBS at a shear rate of 150 s^{-1}. Platelet count was 2.0 × $10^4/\mu$L, and the count of the nanosheets or microparticles was 2.0 × $10^4/\mu$L. *$P < 0.05$ for H12-PLGA nanosheets or H12-PLGA microparticles group vs PBS group. (B) Images of platelet thrombi on a collagen surface after 300 s flow of the imitation thrombocytopenia blood in the presence of (a) PBS, (b) H12-PLGA nanosheets, and (c) H12-PLGA microparticles. (C) Number of platelet thrombi on the collagen surface and mean area of one thrombus based on images of (B). (D,E) SEM images of platelet thrombi involving H12-PLGA nanosheets and H12-PLGA microparticles, respectively. Arrows in the SEM images indicate nanosheets and microparticles.

(*39*). Decuzzi et al. reported on the adhesive strength of ellipsoidal particles toward endothelial cells under a linear shear flow (*40*). They found that ellipsoidal particles adhered more effectively to the cells than classical spherical particles with the same volume because of multivalent bonding of ellipsoidal particles to the cells, and that the adhesive strength was significantly increased by increasing the particle aspect ratio from 1 to 10. On the basis of these studies, we estimate that the high adhesive rate of the H12-PLGA nanosheets is due to an aspect ratio of approximately 20 for the nanosheet. Such a thin sheet can easily flow in the near-wall region (collagen surface) of the flow chamber. The asymmetric shape of the sheets also produces a higher adhesive strength than the spherical microparticles. These experiments clearly demonstrate that the adhesive rate of the carriers on the collagen surface could be controlled solely by changing their shape.

On the other hand, neither carrier adhered to the surface when the platelet count in the blood was below (5.0 ± 1.0) × $10^3/\mu$L (data not shown). Furthermore, both control carriers (without the H12 modification) failed to adhere to the surface (Figure 4). This indicated that the adhesion of the both H12-conjugated carriers was triggered by a specific interaction with the activated platelets, which had already adhered on the surface of the collagen plate. Additionally, we also tried to perform the same flow experiment using 5 by 10 μm rectangular H12-PLGA nanosheets having a very high aspect ratio of over 60 (Supporting Information Figure S3). However, these nanosheets did not adhere to the collagen surface even when H12 was well-conjugated and the shear rate was low (10 s^{-1}) (Supporting Information movie S2). We speculate that this failure to adhere was because it was difficult for these larger nanosheets, together with erythrocytes, to flow in the near-wall region of the flow chamber, and hence they, then did not attach to the activated platelets on the collagen surface. At present, we can say that the platelet-like disk-shaped PLGA-nanosheets with a size of 3 μm have an optimal size and aspect ratio.

Next, in order to know whether the H12-PLGA nanosheets actually have the ability to reinforce platelet thrombus formation under flow conditions, we employed platelets, with an adjusted platelet count of 2.0 × $10^4/\mu$L, were labeled with the fluorescent marker, $DiOC_6$. With the addition of PBS as a control, the flowing platelets gradually adhered to and aggregated on the collagen surface; the surface coverage of platelets after flowing for 300 s increased to 4.7 ± 1.6% as shown in Figure 5A (■) and B (a). When the H12-PLGA nanosheets were added instead of PBS to the thrombocytopenic blood, the surface coverage after 300 s flow was significantly higher at 14.6 ± 1.9% (Figure 5A (○) and B (b)). Furthermore, we confirmed that H12-PLGA nanosheets labeled with rhodamine were involved in the platelet thrombi labeled with $DiOC_6$ by a double-staining method (data not shown). These data indicate that the H12-PLGA nanosheets were specifically bound on the activated platelets adhered on

the collagen surface, and that the number of the H12 peptides on the nanosheets would be sufficient to act as binding sites for the flowing platelets. In case of the H12-PLGA microparticles, their surface coverage was also significantly higher (6.6 ± 1.3%) than that of PBS; however, their effect was lower than that of H12-PLGA nanosheets (Figure 5A (Δ) and B (c)).

In order to clarify the reason the H12-PLGA nanosheets had a more pronounced effect on platelet aggregation than did H12-PLGA microparticles, we calculated the mean area of one platelet thrombus. The numbers of platelet thrombi formed on the collagen surface after 300 s flow were almost comparable in each experiment (PBS, $(7.2 \pm 1.1) \times 10^2/mm^2$; H12-PLGA nanosheets, $(8.1 \pm 1.7) \times 10^2/mm^2$; and H12-PLGA microparticles, $(7.5 \pm 2.1) \times 10^2/mm^2$) (Figure 5C (○)). On the basis of the total area of platelet thrombi, the mean area of one platelet thrombus with the addition of PBS as a negative control was calculated to be $6.1 \pm 1.2\ \mu m^2$. In the presence of the nanosheets, it was interestingly to note that the mean area was significantly increased to $16.6 \pm 2.3\ \mu m^2$ (Figure 5C). The mean area in the presence of the H12-PLGA microparticles was also significantly higher than that of the PBS control at $8.9 \pm 0.7\ \mu m^2$, although this value was significantly lower than that of H12-PLGA nanosheets. This indicates that the H12-PLGA nanosheets make the platelet thrombi spread in a two-dimensional manner.

We also observed with an SEM the surface of the collagen plate after the flow experiments. There were abundant platelet thrombi containing nanosheets or microparticles, where the platelets had adhered first on the collagen surface (Figure 5D,E, respectively). In particular, the H12-PLGA nanosheets two-dimensionally spread the platelet thrombi on the collagen surface, producing a low contrast over the entire SEM image (Figure 5D). On the other hand, the H12-PLGA microparticles made the platelet thrombi pile up dramatically, and the SEM image showed relatively high contrast (Figure 5E). We suggest that the difference may arise from one of the following mechanisms: (1) the adhesion of the both carriers (H12-PLGA nanosheets and H12-PLGA microparticles) could be initiated by the activated platelets, which had already adhered on the surface of the collagen plate, (2) the flat nanosheets adhering to the activated platelets could act as broader scaffolds for binding of the flowing platelets than spherical microparticles, which can only effect point contact with the flowing platelets, or (3) the nanosheets could accelerate two-dimensional platelet thrombus formation because of their ultrathin disk structure, whereas the spherical microparticles would naturally tend to lead to the formation of piled up thrombi. From the viewpoint of hemostasis, the H12-PLGA nanosheets should be more effectively occluded in the thrombi on the collagen exposed at the bleeding site in comparison with H12-PLGA microparticles. Moreover, the biological implications of platelets that have a distinctive disk-shape may be following: the platelets find it easy to adhere to the collagen at the vascular injury, and then their aggregation is two-dimensionally accelerated.

In conclusion, we have successfully prepared biocompatible and biodegradable free-standing, disk-shaped, PLGA nanosheets using patterned ODS/mPEO-SAM, and modified their surfaces with fibrinogen-derived dodecapeptide (H12). The resulting H12-PLGA nanosheets specifically interacted under flow conditions with activated platelets on a collagen surface faster than did H12-PLGA microparticles. Furthermore, the nanosheets, but not the microparticles, induced two-dimensional spreading of platelet thrombi on collagen-immobilized plates. Therefore, H12-PLGA nanosheets might be a suitable candidate as novel platelet substitutes and an alternative to human platelet concentrates infused to treat bleeding in patients with severe thrombocytopenia. We are assessing the *in vivo* hemostatic ability of the H12-PLGA nanosheets to treat animals with severe thrombocytopenia. Moreover, this experimental strategy can be applied to other situation than platelet substitutes, such as other drug delivery carriers like antihemostatic reagents and wound dressings for burn injury, and others.

ACKNOWLEDGMENT

This work was supported as a "Consolidated Research Institute for Advanced Science and Medical Care" and "High-tech Research Center" project by MEXT, Japan (S.T.), and by the Futaba Electronics Memorial Foundation (Y.O.). This work was also supported in part by a Health and Labor Sciences Research Grant (Research on Pharmaceutical and Medical Safety, M.H., Y.I., and S.T.), Ministry of Health, Labor and Welfare, Japan. Y.O. was the recipient of a Research Fellowship from the Japan Health Science Foundation.

Supporting Information Available: Additional figures and movie files as described in the text. This material is available free of charge via the Internet at http://pubs.acs.org.

LITERATURE CITED

(1) Slichter, S. J. (2007) Platelet transfusion therapy. *Hematol. Oncol. Clin. North Am. 21*, 697–729.
(2) Stroncek, D. F., and Rebulla, P. (2007) Platelet transfusions. *Lancet 370*, 427–438.
(3) Graham, S. S., Gonchoroff, N. J., and Miller, J L. (2001) Infusible platelet membranes retain partial functionality of the platelet GPIb/IX/V receptor complex. *Am. J. Clin. Pathol. 115*, 144–147.
(4) Agam, G., and Livine, A. A. (1992) Erythrocytes with covalently bound fibrinogen as a cellular replacement for the treatment of thrombocytopenia. *Eur. J. Clin. Invest. 22*, 105–112.
(5) Casals, E., Verdaguer, A., Tonda, R., Galan, A., Escolar, G., and Estelrich, J. (2003) Atomic force microscopy of liposomes bearing fibrinogen. *Bioconjugate Chem. 14*, 593–600.
(6) Levi, M., Friedrich, P. W., Middleton, S., De Groot, P. G., Wu, Y. P., Harris, R., Biemond, B. J., Heijien, F. G., Levin, J., and Ten Cate, J. W. (1999) Fibrinogen-coated albumin microcapsules reduce bleeding in severely thrombocytopenic rabbits. *Nat. Med. 5*, 107–111.
(7) Coller, B. S., Springer, K. T., Beer, J. H., Mohandas, N., Scudder, L. E., Norton, K. J., and West, S. M. (1992) Thromboerythrocytes. In vitro studies of a potential autologous, semi-artificial alternative to platelet transfusion. *J. Clin. Invest. 89*, 546–555.
(8) Takagi, J., Petre, B. M., Walz, T., and Springer, T. A. (2002) Global comformational rearrangemrents in integrin extracellular domains in outside-in and inside-out signaling. *Cell 110*, 599–611.
(9) Xiao, T., Takagi, J., Coller, B. S., Wang, J. H., and Springer, T. A. (2004) Structual basis for allostery in integrins and binding to fibrinogen-mimetic therapeutics. *Nature 432*, 59–67.
(10) Lam, S. C., Plow, E. F., Smith, M. A., Andrieux, A., Ryckwaert, J. J., Marguerie, G., and Ginsberg, M. H. (1987) Evidence that arginyl-glycyl-aspartate peptides and fibrinogen γ chain peptides share a common binding site on platelets. *J. Biol. Chem. 262*, 947–950.
(11) Andrieux, A., Hudry-Clergeon, G., Ryckewaert, J. J., Chapel, A., Ginsberg, M. H., Plow, E. F., and Marguerie, G. (1989) Amino acid sequences in fibrinogen mediating its interaction with its platelet receptor, GPIIbIIIa. *J. Biol. Chem. 264*, 9258–9265.
(12) Ruoslahti, E. (1996) RGD and other recognition sequences for integrins. *Annu. Rev. Cell Dev. Biol. 12*, 697–715.
(13) Takeoka, S., Teramura, Y., Okamura, Y., Tsuchida, E., Handa, M., and Ikeda, Y. (2002) Rolling properties of rGPIbα-conjugated phospholipid vesicles with different membrane flex-

ibilities on vWf surface under flow conditions. *Biochem. Biophys. Res. Commun. 296*, 765–770.
(14) Okamura, Y., Maekawa, I., Teramura, Y., Maruyama, H., Handa, M., Ikeda, Y., and Takeoka, S. (2005) Hemostatic effects of phospholipid vesicles carrying fibrinogen-γ chain dodecapeptide in vitro and in vivo. *Bioconjugate Chem. 16*, 1589–1596.
(15) Okamura, Y., Takeoka, S., Eto, K., Maekawa, I., Fujie, T., Maruyama, H., Ikeda, Y., and Handa, M. (2009) Development of fibrinogen γ-chain peptide-coated, adenosine diphosphate-encapsulated liposomes as a synthetic platelet substitute. *J. Thromb. Haemost. 7*, 470–477.
(16) Takeoka, S., Teramura, Y., Okamura, Y., Handa, M., Ikeda, Y., and Tsuchida, E. (2001) Fibrinogen-conjugated albumin polymers and their interaction with platelets under flow conditions. *Biomacromolecules 2*, 1192–1197.
(17) Teramura, Y., Okamura, Y., Takeoka, S., Kainoh, M., Narumi, H., Tsuchiyama, H., Handa, M., Ikeda, Y., and Tsuchida, E. (2003) Hemostatic effects of polymerized albumin particles bearing rGPIa/IIa in thrombocytopenic mice. *Biochem. Biophys. Res. Commun. 306*, 256–260.
(18) Okamura, Y., Takeoka, S., Teramura, Y., Maruyama, H., Tsuchida, E., Handa, M., and Ikeda, Y. (2005) Hemostatic effects of fibrinogen γ-chain dodecapeptide-conjugated polymerized albumin particles in vitro and in vivo. *Transfusion 45*, 1221–1228.
(19) Okamura, Y., Fujie, T., Maruyama, H., Handa, M., Ikeda, Y., and Takeoka, S. (2007) Prolonged hemostatic ability of poly(ethylene glycol)-modified polymerized albumin particles carrying fibrinogen γ-chain dodecapeptide. *Transfusion 47*, 1254–1262.
(20) Okamura, Y., Fujie, T., Nogawa, M., Maruyama, H., Handa, M., Ikeda, Y., and Takeoka, S. (2008) Hemostatic effects of polymerized albumin particles carrying fibrinogen γ-chain dodecapeptide as platelet substitutes in severely thrombocytopenic rabbits. *Transf. Med. 18*, 158–166.
(21) Mattson, J., Forrest, J. A., and Borjesson, L. (2000) Quantifying glass transition behaviour in ultrathin free-standing polymer films. *Phys. Rev. E 62*, 5187–5200.
(22) Tang, Z., Kotov, N. A., Magonov, S., and Ozturkk, B. (2003) Nanostructured artificial nacre. *Nat. Mater. 2*, 413–418.
(23) Mallwitz, F., and Laschewsky, A. (2005) Direct access to stable, freestanding polymer membranes by layer-by-layer assembly of polyelectrolytes. *Adv. Mater. 17*, 1296–1299.
(24) Fujie, T., Okamura, Y., and Takeoka, S. (2007) Ubiquitous transference of free-standing polysaccharide nanosheet in the development of a nano-adhesive plaster. *Adv. Mater. 19*, 3549–3553.
(25) Mallwitz, F., and Goedel, W. A. (2001) Physically cross-linked ultrathin elastomeric membranes. *Angew. Chem., Int. Ed. 40*, 2645–2647.
(26) Eck, W., Küller, A., Grunze, M., Völkel, B., and Gölzhäuser, A. (2005) Freestanding nanosheets from crosslinked biphenyl self-assembled monolayers. *Adv. Mater. 17*, 2583–2587.
(27) Ulman, A. (1991) *An introduction to ultrathin organic films from langmuir-blodgett to self-assembly*, Academic Press, San Diego, CA.
(28) Niwa, D., Yamada, Y., Homma, T., and Osaka, T. (2004) Formation of molecular templates for fabricating on-chip biosensing devices. *J. Phys. Chem. B 108*, 3240–3245.
(29) Khoshtariya, D. E., Wei, J., Liu, H., Yue, H., and Waldeck, D. H. (2003) Charge-transfer mechanism for cytochrome *c* adsorbed on nanometer thick films. Distinguishing frictional control from conformational gating. *J. Am. Chem. Soc. 125*, 7704–7714.
(30) Ferapontova, E. E., Shipovskov, S., and Gorton, L. (2007) Bioelectrocatalytic detection of theophylline at theophylline oxidase electrodes. *Biosens. Bioelectron. 22*, 2508–2511.
(31) Sun, Y., and Walker, G. C. (2002) Two-dimensional self-assembly of latex particles in wetting films on patterned polymer. *J. Phys. Chem. B 106*, 2217–2223.
(32) Okamura, Y., Utsunomiya, S., Suzuki, H., Niwa, D., Osaka, T., and Takeoka, S. (2008) Fabrication of freestanding nanoparticle-fused sheets and their hetero-modification using sacrificial film. *Colloids Surf., A 318*, 184–190.
(33) Sugimura, H., Ushiyama, H., Hozumi, A., and Takai, O. (2000) Micropatterning of alkyl- and fluoroalkylsilane self-assembled monolayers using vacuum ultraviolet light. *Langmuir 16*, 885–888.
(34) Cecchet, F., Meersman, B. D., Demoustier-Champagne, S., Nysten, B., and Jonas, A. M. (2006) One step growth of protein antifouling surface: monolayers of poly(ethylene oxide) (PEO) derivatives on oxdized and hydrogen-passivated silicon surfaces. *Langmuir 22*, 1173–1181.
(35) Ravi Kumar, M. N. V., Bakowsky, U., and Lehr, C. M. (2004) Preparation and characterization of cationic PLGA nanospheres as DNA carriers. *Biomaterials 25*, 1771–1777.
(36) Sahoo, S. K., Panyam, J., Prabha, S., and Labhasetwar, V. (2002) Residual polyvinyl alcohol associated with poly(d,l-lactide-co-glycolide) nanoparticles affects their physical properties and cellular uptake. *J. Controlled Release 82*, 105–14.
(37) Denkov, N. D., Velev, O. D., Kralchevsky, P. A., Ivanov, I. B., Yoshimura, H., and Nagayama, K. (1992) Mechanism of formation of two-dimensional crystals from latex particles on substrates. *Langmuir 8*, 3183–3190.
(38) Stroock, A. D., Kane, R. S., Weck, M., Metallo, S. J., and Whitesides, G. M. (2003) Synthesis of free-standing quasi-two-dimensional polymers. *Langmuir 19*, 2466–2472.
(39) Mortensen, P. H., Andersson, H. I., Gillissen, J. J. J., and Boersma, B. J. (2008) On the orientation of ellipsoidal particles in a turbulent shear flow. *Int. J. Multiphase Flow 34*, 678–683.
(40) Decuzzi, P., and Ferrari, M. (2006) The adhesive strength of non-spherical particles mediated by specific interactions. *Biomaterials 27*, 5307–5314.

BC900325W

Fabrication of free-standing albumin-nanosheets having heterosurfaces

Yosuke Okamura, Takahiro Goto, Daisuke Niwa, Yoshihito Fukui, Masanobu Otsuka, Norikazu Motohashi, Tetsuya Osaka, Shinji Takeoka

Consolidated Research Institute for Advanced Science and Medical Care, Waseda University, Tokyo 169-8555, Japan

Received 2 August 2007; revised 11 December 2007; accepted 11 December 2007
Published online 22 April 2008 in Wiley InterScience (www.interscience.wiley.com). DOI: 10.1002/jbm.a.31934

Abstract: Sheet-shaped carriers, having both obverse and reverse surfaces and thus a large contact area for targeting a site, have several advantages over spherical-shaped carriers, which have an extremely small contact area for targeting sites. Here, we proposed a novel method to prepare a free-standing ultrathin and biocompatible nanosheet having heterosurfaces, by a combination of four processes: (1) specific adsorption of recombinant human serum albumin (rHSA) molecules onto a patterned octadecyltrimethoxysilane self-assembled monolayer region (ODS-SAM), (2) preparation of nanosheets of rHSA molecules bearing thiol groups (SH-rHSA) via two-dimensionally disulfide crosslinking, (3) surface modification of the resulting nanosheet, and (4) preparation of the free-standing nanosheet by detachment from the ODS-SAM. The SH-rHSA molecules at pH 5.0 and a concentration of 1 μg/mL were specifically adsorbed on the patterned ODS-SAM regions by hydrophobic interaction, and were two-dimensionally crosslinked in the presence of copper ion as an oxidant. The rHSA-nanosheets were then simply detached from the ODS-SAM by treatment with surfactant. We succeeded in the preparation of rectangular (10 μm × 30 μm) and ultrathin (4.5 ± 1.0 nm) rHSA-nanosheets on a patterned ODS-SAM, and could also obtain free-standing rHSA-nanosheets having heterosurfaces by surface modification with fluorescent latex beads. Thus, the rHSA-nanosheets having heterosurfaces could be regarded as a new biomaterial for drug carriers, hemostatic reagents, wound dressing for burn injury, and so forth. © 2008 Wiley Periodicals, Inc. J Biomed Mater Res 89A: 233–241, 2009

Key words: albumin; nanosheet; free-standing; biocompatibility; crosslinking

INTRODUCTION

In recent years, much attention has been paid to drug-delivery system (DDS) as a new pharmacological approach to improve the efficacy and safety of drugs. In DDS, vesicles, micelles, emulsions, and biodegradable nanoparticles have been extensively studied as carriers for biologically active substances such as drugs, recognition proteins, enzymes, genes, and so forth.[1] There are two concepts for the development of DDS: passive and active targeting systems. In the latter case, recognition proteins such as antibodies and various ligands are conjugated to the surface of the carriers to target the tissue epitopes or specific cells.

We have developed biocompatible and biodegradable nanoparticles such as albumin-based nanoparticles[2–5] and phospholipid vesicles[6,7] carrying recombinant fragments of platelet membrane proteins[3,4,6,8] and dodecapeptide as a recognition site for fibrinogen.[2,5,7,9] These nanoparticles specifically recognized the site of bleeding injury or activated platelets. In our approach to the conjugation of high- and low-molecular-weight molecules such as glycoprotein Ibα and dodecapeptide to the surface of the particle, we observed that the activity of dodecapeptide was suppressed by the steric hindrance of the glycoprotein Ibα, and found that a spacer such as a poly(ethylene glycol) chain was needed in the conjugation of the peptides.[8]

On the other hand, sheet-shaped carriers, having both obverse and reverse surfaces and thus a large contact area for targeting a site, have several advantages over spherical-shaped carriers, which have an extremely small contact area for targeting sites. Recently, several approaches have been implemented for the fabrication of free-standing films, combining large surface area with nanoscale thickness, from polymers and/or from inorganic materials: cast films,[10] layer-by-layer assemblies of polyelectolyte multilayers,[11–15] crosslinked amphiphilic Langmuir–Blodgett films,[16] self-assembled monolayers (SAMs),[17,18] and assemblies of triblock copolymers.[19] However, there

Correspondence to: S. Takeoka; e-mail: takeoka@waseda.jp
Contract grant sponsor: Shorai Foundation for Science and Technology

have been no reports on the preparation of free-standing nanoscale sheets from biocompatible and biodegradable materials only. The nanosheets would be a candidate as a new injectable biomaterial in DDSs.

Organosilane SAMs have been widely applied to control physical and chemical properties of the surfaces of glass, quartz, SiO_2/Si wafers, or silica particles.[20] Furthermore, they are excellent tools to study the immobilization of proteins such as redox proteins,[21] enzymes,[22] and immunoglobulins, using covalent bonds or noncovalent bonds such as ionic or hydrogen bonds, van der Waals attraction, and hydrophobic interaction with the various terminal groups of SAMs. Generally, it is easy to construct patterned SAMs with uniform sizes and shapes on silicon oxide or gold substrates using conventional photolithography processes.[23] This approach was used for the electrochemical analysis of proteins immobilized by adsorption on the substrates.

Here, we proposed a novel method to prepare a free-standing biocompatible nanosheet having heterosurfaces. We used a patterned hydrophobic octadecyltrimethoxysilane-SAM (ODS-SAM) on silicon oxide to prepare nanosheets of uniform sizes and shapes. Furthermore, we modified the surface of the nanosheet with fluorescent latex beads as a model material to prove the fabrication of a nanosheet with heterosurfaces.

MATERIALS AND METHODS

Reagents

P-type Si (100) wafers (below 0.02 Ω cm) covered with thermally grown silicon oxide (~200 nm) was purchased from KST World, Co. (Fukui, Japan). *n*-Octadecyltrimethoxysilane (ODS, 97%) was purchased from Gelest (Morrisville, PA). Succinimidyl 6-[3′-(2-pyridyldithio) propionamido] hexanoate (LC-SPDP) and *N*-(ε-maleimidocaproyl) succinimide ester (EMCS) were purchased from Pierce Biotechnology (Rockford, IL). Dithiothreitol (DTT) and copper sulfate pentahydrate were purchased from Wako Pure Chemical Industries (Osaka, Japan). 5,(6)-Tetramethylrhodamine isothiocyanate (TRITC) and 7-chloro-4-nitrobenzo-2-oxa-1,3-diazole (NBD) were purchased from Invitrogen (Carlsbad, CA). Sephadex G25 for gel permeation chromatography (GPC) was purchased from GE Healthcare UK (Buckinghamshire, England). Latex beads (Polybead™, 100 nm ϕ) were purchased from Polysciences (Warrington, PA). Recombinant human serum albumin (rHSA, 250 mg/mL) was kindly donated by Oxgenix Co. (Tokyo, Japan).

SAM preparation

Silicon wafers were treated with SPM (96% H_2SO_4: 30% H_2O_2 = 4:1 (v/v)) at 120°C followed by rinsing with distilled water. The resulting wafers were placed in a 20-mL Teflon vial containing a glass cup filled with 200 μL of ODS liquid. The vials were sealed with a cap and then heated for 8 h at a constant temperature of 110°C in a dry room to prepare a hydrophobic ODS-SAM on the silicon oxide.[24]

Patterning processes

The patterned ODS-SAM having hydrophobic octadecyl regions and hydrophilic silicon oxide regions on the substrate was prepared by a conventional photolithography process. The ODS-SAM on the silicon oxide was covered with a photoresist (OFPR-800 500 cP, Tokyo Ohka Kogyo, Co., Kanagawa, Japan), and was irradiated with a 350-nm UV lamp (MA-10, Mikasa, Tokyo, Japan) using a photomask (size: 1 cm × 1 cm, patterning; rectangle (10 μm × 30 μm), Topic Co., Saitama, Japan). After developing (NMD-3), the substrate was exposed to oxygen plasma (Plasma Reactor PR301, Yamato Scientific Co., Tokyo, Japan) at an input power of 200 W and an oxygen flow rate of 80 sccm for removal of ODS. The photoresist was removed by acetone washing to obtain the patterned ODS-SAM.

Contact angle measurements

A 3-μL drop of distilled water was placed directly onto the ODS-SAM with a micropipette before and after rHSA adsorption, or after the addition of surfactant as described earlier. The liquid drops were observed with an optical microscope with 5× magnification. All water contact angles represented the mean ± SD of the five measurement values.

Chemical modification of rHSA with thiol groups

An rHSA solution (250 mg/mL) was diluted to 50 mg/mL with a phosphate buffer solution (pH 7.4). A 50 m*M* solution of LC-SPDP in DMSO (150 μL) was added to the rHSA solution (1 mL), and the solution was incubated for 20 min at r.t. To the rHSA solution, a 10 m*M* TRITC phosphate buffer solution (112.5 μL, pH 7.4) was then added and incubated for 20 min at r.t. The unreacted LC-SPDP (precipitated), TRITC, and the byproducts were separated by centrifugation, and then by GPC with an acetate buffer (pH 5.0) to obtain a pyridyl disulfide-bearing rHSA (PD-rHSA). DTT [final concentration (f.c.) 20 m*M*] was added to the PD-rHSA solution to reduce the PD group to a SH group. The unreacted DTT and the byproducts were separated by GPC with an acetate buffer (pH 5.0), and the fractions of TRITC-labeled thiol-introduced rHSA (TRITC-labeled SH-rHSA) were collected. The number of the SH groups conjugated to one rHSA molecule was determined by the quantification of the 2-thiopyridone (2-TP) at 343 nm that was liberated by the addition of DTT.

Preparation of rHSA-nanosheets

As shown in Figure 1, the substrate of the patterned ODS-SAM was immersed into an acetate buffer solution

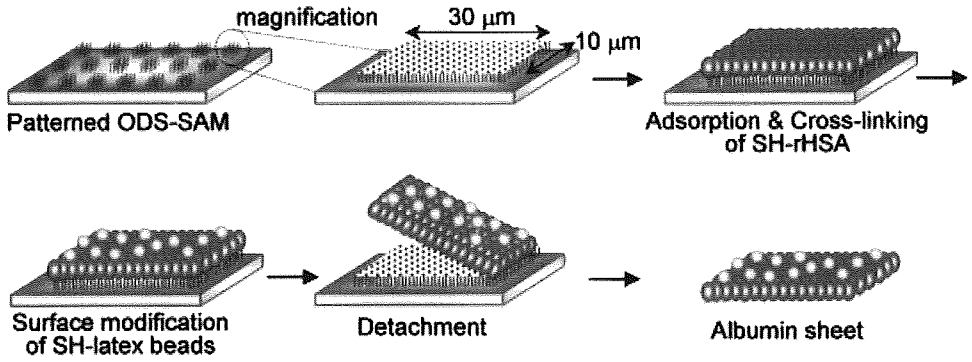

Figure 1. Preparation of free-standing rHSA-nanosheets having heterosurfaces on the patterned ODS-SAM. [Color figure can be viewed in the online issue, which is available at www.interscience.wiley.com.]

(pH 5.0) of the TRITC-labeled SH-rHSA at a concentration of 1 μg/mL for 1 h at r.t., and washed with an acetate buffer solution to remove the nonadsorbed SH-rHSA. The substrate was immersed into an acetate buffer solution containing copper ion (II) as a catalyst[25] at a concentration of 1 μ*M* for 12 h at r.t. The series of adsorption, crosslinking, and washing processes were repeated three times. The substrate was immersed into a 1% (v/v) deca(oxyethylene) dodecyl ether ($C_{12}E_{10}$) solution at r.t. for 6 h, to obtain a free-standing rHSA-nanosheet suspension by releasing the rHSA-nanosheets from the substrate. We observed the resulting rHSA-nanosheets using an epifluorescence microscope (ECLIPS TE300, Nikon Co., Tokyo, Japan) equipped with a CCD camera, a confocal laser scanning microscope (LSM 510, Zeiss, Nikon Co.), and an atomic force microscope (AFM) at a tapping mode with a MFP-3D-BIO (Asylum Research, Co., Santa Barbara, CA).

Conjugation of NBD-labeled latex beads to the surface of rHSA-nanosheets

Latex beads (ϕ 100 nm) were mixed with an rHSA solution (50 mg/mL) and incubated at r.t. for 2 h to coat the surface of the latex bead with rHSA. After the separation of the free rHSA by ultracentrifugation (100,000*g*, 10 min, 4°C, twice), the rHSA-coated latex beads (rHSA-latex beads) were dispersed in a phosphate buffer solution (pH 7.4). The amount of rHSA adsorbed on the surface of the latex bead was analyzed by a microBCA kit (Pierce Biotechnology). A solution of LC-SPDP in DMSO (2 eq. mol with respect to the rHSA adsorbed on the surface of the latex bead) was added to the suspension of the rHSA-latex beads and incubated for 20 min at r.t. The solution of NBD in DMSO (2 eq. mol with respect to rHSA on the surface of the latex bead) was added to the suspension and incubated for 20 min at r.t. A DTT treatment (f.c. 20 m*M*) was carried out to reduce the PD groups to SH groups. The unreacted DTT and byproducts were separated by GPC, and the NBD-labeled thiol-bearing latex beads [SH-(NBD)latex beads] were collected.

On the other hand, the substrate of the TRITC-labeled rHSA-nanosheets was immersed in a phosphate buffer, and a DMSO solution of EMCS was added to the substrate and incubated for 20 min at r.t. to introduce maleimido groups on the nanosheet. The unreacted EMCS and byproducts were washed with a phosphate buffer, and the maleimido-bearing rHSA-nanosheets were obtained.

Finally, the SH-(NBD)latex beads were added to the maleimido-bearing rHSA-nanosheets, and incubated for 2 h at r.t. The unreacted SH-(NBD)latex beads and byproducts were washed with a phosphate buffer, and the rHSA-nanosheets, of which the obverse side was modified with the NBD-labeled latex beads, were observed using a confocal laser scanning microscope (LSM 510) and a Hitachi S-4500 field emission scanning electron microscope (SEM).

RESULTS

Water contact angle

The water contact angle of the substrate, which was coated with ODS-SAM, was estimated to be 83° ± 1° as listed in Table I. When the ODS-SAM-coated substrate was immersed into a phosphate buffer solution (pH 7.4) of rHSA at a concentration of 100 μg/mL, the water contact angle did not change (80° ± 2°). However, when the substrate was immersed in an acetate buffer solution (pH 5.0) of rHSA, the angle was significantly decreased to 67° ± 1°. The angle was restored to 82° ± 1° when the rHSA-treated substrate was immersed into a 1% (v/v) solution of $C_{12}E_{10}$ for 1 h. Therefore, we confirmed

TABLE I
Water Contact Angles of ODS-SAM Before and After rHSA Adsorption

rHSA Adsorption	Water Contact Angle (degree)
Before	83 ± 1
After	
pH 5.0	67 ± 1
pH 7.4	80 ± 2
$C_{12}E_{10}$[a]	82 ± 1

[a] $C_{12}E_{10}$ was added to the ODS-SAM after rHSA adsorption at pH 5.0, incubated at r.t. for 1 h and then washed with distilled water.

that rHSA molecules were adsorbed on the ODS-SAM at pH 5.0, and the adsorbed rHSA molecules were detached from the substrate by surfactant treatment.

Preparation of rHSA-nanosheets

We could not analyze the crosslinking ratio of the SH-rHSA molecules adsorbed on the ODS-SAM from quantification of the unreacted SH groups of the rHSA, because the amount of the adsorbed rHSA was below the detection limit. We explored the crosslinking of the SH-rHSA in an aqueous solution in order to determine the extent of crosslinking of the SH-rHSA on the ODS-SAM. We determined the number of SH groups bound to one rHSA molecule for mixtures of LC-SPDP and rHSA at 5, 7, and 10 mol/mol (mole equivalent of the rHSA concentration) ratios of LC-SPDP to rHSA. Based on the quantification of the 2-TP liberated by the addition of DTT, the number of SH groups bound to one rHSA molecule was estimated to be $\sim 2.9 \pm 0.8$, 4.7 ± 1.1, and 7.4 ± 1.2 molecules, respectively. We oxidized the SH-rHSA molecules in the presence of copper ion (II) at r.t. and measured the degree of reaction by HPLC with a TSK-GEL G4000SW$_{XL}$ column, by measuring the absorbance of the column effluent at 220 nm, which was attributed to the absorption of the amide linkage of rHSA. At pH 5.0, the three kinds of SH-rHSA having different numbers of SH groups were crosslinked, and the percentage of the peak area of the void fraction to the total peak, which corresponded to the amount of the crosslinked rHSA with a molecular weight of >670 kDa based on the elution time of thyroglobulin as a marker protein, was increased to 64, 75, and 96% with the increasing number of the SH groups bound to one rHSA molecule. All reactions were completed within 12 h. On the other hand, the three kinds of SH-rHSA were hardly crosslinked in the absence of copper ion (II) at pH 5.0 or in the presence of copper ion (II) at pH 7.4. Based on the earlier results, we decided that SH-rHSA molecules with 7.4 ± 1.2 SH groups bound to one rHSA molecule were to be crosslinked on the patterned ODS-SAM at pH 5.0 for 12 h in the presence of 1 μM copper ion (II).

Next, we explored the adsorption of SH-rHSA on the rectangle-patterned ODS-SAM regions. When the substrate of the patterned ODS-SAM was immersed in an acetate buffer solution (pH 5.0) of the TRITC-labeled SH-rHSA at a concentration of 1 μg/mL, the rectangular patterns (10 μm × 30 μm) were completely and selectively stained by the TRITC-labeled SH-rHSA as shown in Figure 2(a). After removing the nonadsorbed SH-rHSA by washing with the acetate buffer solution, we crosslinked the SH-rHSA molecules adsorbed on the patterned ODS-SAM following the aforementioned conditions, and immersed the substrate in a 1% $C_{12}E_{10}$ solution at r.t. for 6 h to detach the rectangles from the substrate. Next, we dropped the $C_{12}E_{10}$ solution containing the rectangular sheets onto a glass plate, and observed the surface of the plate using a confocal laser scanning microscopy. There were abundant rectangular rHSA-nanosheets in various conformations; in particular, the bent form of the rHSA-nanosheets was successfully observed in the three-dimensional images [Fig. 2(b,c)], demonstrating the flexible and tough nature of the rHSA-nanosheets.

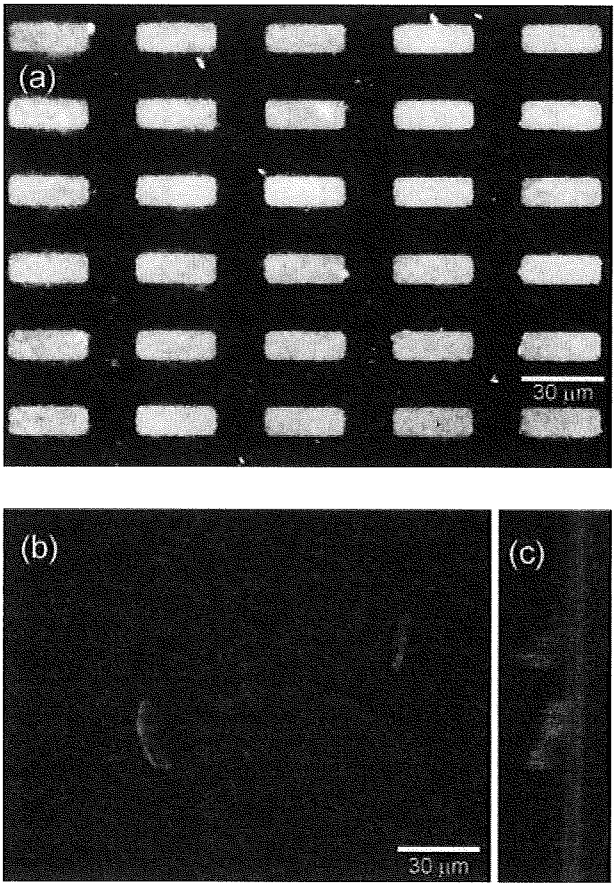

Figure 2. (a) Observation of SH-rHSA adsorbed onto the patterned ODS-SAM using fluorescent microscopy. (b) Observation of the free-standing rHSA-nanosheets detached from the patterned ODS-SAM and (c) the 90° rotation image of (b) using confocal laser fluorescent microscopy.

AFM analysis of rHSA-nanosheets

To establish the morphological detail and the thickness of the rHSA-nanosheets, the nanosheets on the patterned ODS-SAM were observed by AFM. Figure 3(a) shows a large-scale (90 μm × 90 μm), three-dimension AFM image of the rHSA-nano-

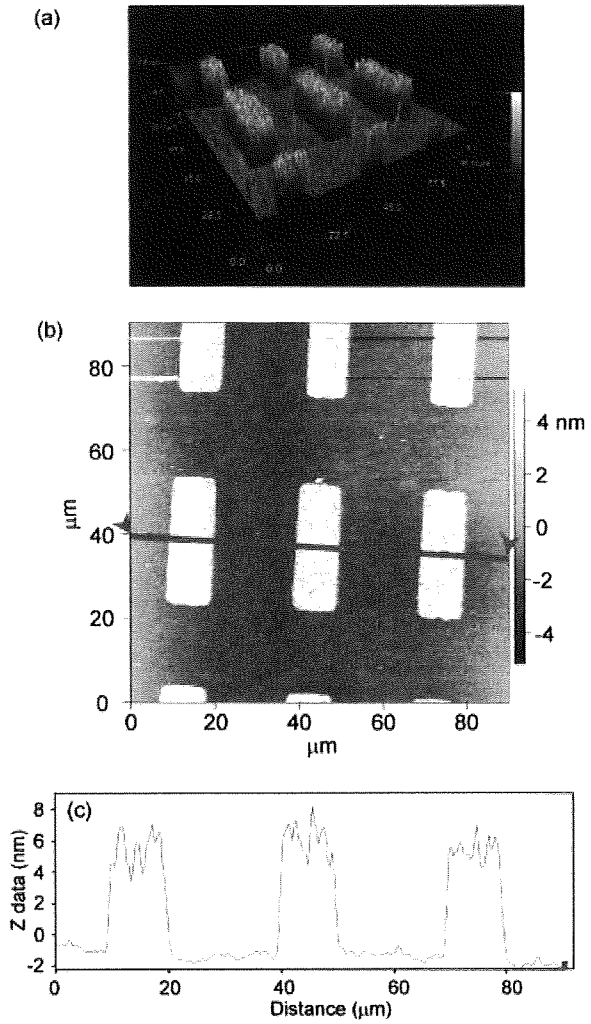

Figure 3. AFM images of rHSA-nanosheets adsorbed onto the patterned ODS-SAM. (a) 3-D image, (b) top view image, and (c) cross-sectional image. [Color figure can be viewed in the online issue, which is available at www.interscience.wiley.com.]

sheets. The rectangular patterns (10 μm × 30 μm) were vividly embossed by rHSA, and nonspecific adsorption of rHSA was scarcely observed on the SiO_2 regions. From the AFM cross-sectional image, the thickness of the rHSA-nanosheets plus the ODS-SAM was estimated to be 6.6 ± 1.0 nm as shown in Figure 3(b,c). On the other hand, the thickness of the ODS-SAM itself was estimated to be 2.1 ± 0.7 nm (data not shown). Based on the difference between both thicknesses, the thickness of the rHSA-nanosheets was calculated to be 4.5 ± 1.0 nm, which agrees with the dimensions of rHSA.

rHSA-nanosheets having heterosurfaces

For fabrication of the rHSA-nanosheets having heterosurfaces, we conjugated NBD-labeled latex beads to the obverse side of TRITC-labeled rHSA-nanosheets on ODS-SAM. After the rHSA-nanosheets were detached from the ODS-SAM by the surfactant treatment, the dispersion was put on the cover glass plate, and then the sheets were observed with a confocal laser scanning microscope. There were abundant rectangular rHSA-nanosheets in various conformations (10 μm × 30 μm). We focused on a sheet adopting a bent form as shown in Figure 4. When the rhodamine-labeled rHSA of the sheets was excited at 543 nm, the entire sheet turned red with a measured emission wavelength of over 570 nm as shown in Figure 4(a). On the other hand, NBD of the latex beads was excited at a wavelength of 458 nm and detected in the emission wavelength region from 500 to 530 nm. We observed that the majority of the surface of the sheets turned yellow, and the bent site of the nanosheet was quenched due to the fluorescent resonance energy transfer (FRET) effect from the NBD to the rhodamine as shown in Figure 4(b). When these pictures (a) and (b) were overlayed, the resulting picture (c) clearly showed the red and yellow heterosurfaces, suggesting that NBD-labeled latex beads adhered to the reverse surface at the bent site of the rHSA-nanosheet. Finally, we observed the latex beads-conjugated rHSA-nanosheets on ODS-SAM using an SEM. Many latex beads were specifically conjugated to the obverse side of the rHSA-nanosheets. The contrast of the rHSA-nanosheet was clear and uniform in comparison with that of SiO_2 region as shown in Figure 4(e,f), suggesting that the rHSA-nanosheets were thin and flat.

DISCUSSION

The purpose of this article is to propose a novel method to prepare free-standing biocompatible nanosheets having heterosurfaces, as a new biomaterial, by a combination of four processes as shown in Figure 1: (1) specific adsorption of rHSA molecules onto patterned hydrophobic ODS-SAM regions, (2) preparation of nanosheets of SH-rHSA via two-dimensionally disulfide crosslinking, (3) surface modification of the resulting nanosheets, and (4) preparation of free-standing nanosheets by detachment from the ODS-SAM.

We selected hydrophobic ODS having a terminal CH_3 group for the SAM. Wadu-Mestheige et al. reported that bovine serum albumin could be selectively adsorbed on the SAM regions having a terminal CH_3 in comparison with SAM regions having a terminal OH or COOH.[26] Since the resulting water contact angle of the ODS-SAM was similar to that of the ODS-SAM in the previous reports,[27,28] we could confirm that the hydrophobic ODS-SAM was certainly constructed on the silicon oxide (Table I).

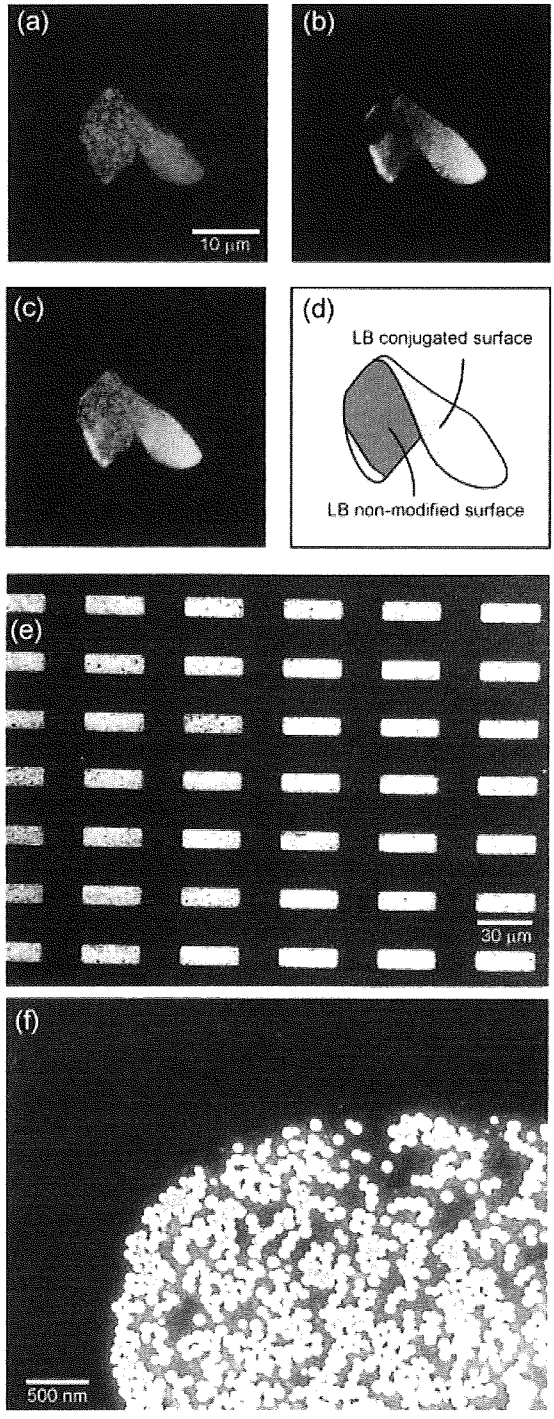

Figure 4. Confocal laser scanning microscopic images of rhodamine-labeled rHSA-nanosheets, of which the obverse sides were modified with NBD-labeled latex beads. (a) Rhodamine-conjugated rHSA was excited at a wavelength of 543 nm, and the emission wavelength detected at over 570 nm, (b) NBD conjugated latex beads were excited at a wavelength of 458 nm and the emission wavelength detected at 500–530 nm, (c) the overlayed image of (a) and (b), and (d) Schematic image of rhodamine-labeled rHSA-nanosheets, of which the obverse sides were modified with NBD-labeled latex beads. (e) SEM image of rHSA-nanosheets, of which the obverse sides were modified with latex beads. (f) Magnified SEM image of (e).

As a first step, we investigated the suitable conditions (pH and concentration) for rHSA adsorption onto the ODS-SAM. At pH 7.4, the rHSA molecules did not adsorb on the ODS-SAM, as seen from the contact angle measurement (Table I). At that pH, the charge of rHSA is negative, because the isoelectric point of rHSA is 4.9. Above that pH, rHSA molecules have little hydrophobic interaction with ODS-SAM and repel each other electrostatically. Therefore, they favor remaining dissociated in the solution rather than to assemble onto the ODS-SAM, resulting in no change in the contact angle. At pH 5.0, near the isoelectric point of rHSA, the contact angle was significantly decreased, suggesting that the rHSA molecules were firmly adsorbed on the ODS-SAM. As described later in the final step, the water contact angle after the surfactant treatment was comparable to that of the ODS-SAM before rHSA adsorption, indicating that the attractive force giving rise to the adsorption of rHSA on the ODS-SAM was hydrophobic interaction. These results are consistent with the previous reported experiments on albumin adsorption at pH 5.0 and influences the three-dimensional shape of the individual albumin adsorbed on the terminal CH_3 of SAM.[29,30] These previous studies reported on the adsorption mechanism of albumin onto the SAM as the following: the electrostatic repulsion among albumin molecules was decreased at pH 5.0 and the interprotein interaction (mostly hydrophobic interaction) strengthened, thus the albumin immobilized on the SAM was more stable than individual proteins in the solution state.

Next, at pH 5.0 and r.t., we explored the optimum concentration of the TRITC-labeled SH-rHSA adsorbed on the patterned ODS-SAM. In the case of the TRITC-labeled SH-rHSA at a concentration of 10 μg/mL or over, the rectangular patterns were distinctly stained by fluorescence; however, the SH-rHSA molecules were nonspecifically adsorbed on the hydrophilic silicon oxide regions and brightened the background (data not shown). In the case of the SH-rHSA at a concentration of 0.1 μg/mL, the ODS patterns were hardly stained (data not shown). At a concentration of 1 μg/mL, almost all the ODS patterns were selectively stained (Fig. 2) and the rHSA molecules were predominantly located in the patterned ODS region (Fig. 3). The number of the ODS patterns arranged on the substrate (1 cm × 1 cm) is estimated to be $\sim 6.7 \times 10^4$, and the number of rHSA molecules adsorbed on one patterned ODS region was calculated to be $\sim 1.2 \times 10^7$ molecules, if the average surface area of one rHSA molecule is 25.5 nm^2,[31] and rHSA molecules are closely packed in the patterned ODS region (rectangular patterns: 10 μm × 30 μm, area: 3.0×10^8 nm^2). Accordingly, the total number of the rHSA molecules adsorbing on the ODS patterns was calculated to be $\sim 8.0 \times 10^{11}$ mole-

cules. Approximately 9% of the total rHSA was estimated to be adsorbed onto the ODS regions by immersing the substrate in the 1 mL rHSA solution at a concentration of 1 μg/mL, containing 9.0×10^{12} rHSA molecules. This was also supported by the results obtained from the other patterns such as circles and squares (data not shown). Consequently, we set the conditions of the rHSA adsorption onto the patterned ODS-SAM, at pH 5.0, at r.t. and the concentration of 1 μg/mL.

The second step of the process is to crosslink each SH-rHSA molecule adsorbed on the patterned ODS-SAM to prepare nanosheets. We presumed that once the SH-rHSA molecules were adsorbed onto the substrate they would closely pack in the pattern, and thus be easy to crosslink in comparison with those in an aqueous solution. We utilized the crosslinking conditions for SH-rHSA in an aqueous solution to estimate the necessary conditions for crosslinking on the ODS-SAM. Crosslinking of the SH-rHSA by *N*-succinimidyl 3-(2-pyridyldithio) propionate (SPDP, spacer length is 0.68 nm), which has a terminal succinimidyl group and a pyridyldisulfide group to introduce the SH group to the surface of rHSA molecule after a DTT treatment, failed probably because the spacer length of SPDP would be too short to crosslink. Referring to a report by Komatsu et al., where a dimer and clusters of rHSA had been exquisitely synthesized using a bis-maleimidohexane and an LC-SPDP, which have spacer lengths of 1.61 and 1.57 nm, respectively,[31,32] we used the LC-SPDP, which has similar functionality as that of SPDP. Only a small proportion of the SH-rHSA molecules crosslink at pH 7.4 in the presence of copper ion (II) as described in a previous report,[25] suggesting that the rHSA molecules electrostatically repel each other because of the negative ζ-potential of the rHSA molecule. At pH 5.0, near the isoelectric point (pI = 4.9), the SH-rHSA was significantly crosslinked. The percentage of the peak areas of the void fractions for the total peak areas, which corresponded to the amount of the crosslinked rHSA over the molecular weight of 670 kDa, increased with the increasing number of the SH groups bound to one rHSA molecule. On the other hand, the crosslinking of the SH-rHSA was extremely slow in the absence of copper ion (II). The thiol oxidation is commonly facilitated in alkaline conditions because of complexation of copper ion (II) with thiolate anions.[25] However, we used the weakly acidic conditions (pH 5.0), where the reaction rate was considered to be slow, suggesting that the thiol oxidation of the rHSA molecules would be controlled by electrostatic repulsion and hydrophobic interaction of rHSA molecules. Based on the earlier results, we could crosslink the SH-rHSA molecules adsorbed on the patterned ODS-SAM at pH 5.0 in the presence of 1 μ*M* copper ion (II).

We measured the thickness of the rHSA-nanosheets as 4.5 ± 1.0 nm from the thickness of the ODS-SAM alone and the rHSA-nanosheet adsorbed on the ODS-SAM using AFM (Fig. 3). Carter and Ho reported that the tertiary structure of the HSA molecule determined from X-ray diffractometry could be described as a heart-shaped or equilateral triangular molecule, with each side 8 nm in length and with an average thickness of 3 nm.[33] The result showed that the rHSA-nanosheets could be regarded as a monolayer of SH-rHSA. As the hydrophobic interaction of SH-rHSA molecules with ODS-SAM should be stronger than that of SH-rHSA molecules with each other, the rHSA molecules weakly adsorbed onto the rHSA monolayer could be removed by washing before the addition of copper ion (II) as a catalyst of disulfide crosslinking. Furthermore, we confirmed that the nonspecific adsorption onto the SiO_2 surface was extremely reduced if the substrate were immersed into the rHSA solution under the aforementioned conditions, based on the results obtained by AFM as well as fluorescent microscopy.

In the third step, we tried to modify the surface of the resulting nanosheet with latex beads, which were useful carriers because of their uniform size and ease of confirmation by microscopic observation. We conjugated the NBD-labeled latex beads onto the obverse side of the TRITC-labeled rHSA-nanosheets that had been adsorbed on the ODS-SAM and demonstrated the preparation of nanosheets having heterosurfaces. As shown in Figure 4, there were many rHSA-nanosheets in various conformations of rectangles, such as bent forms. Surprisingly, there were no broken sheets, suggesting that the rHSA-nanosheets are tough and extremely flexible. Focusing on the nanosheet having a bent form (Fig. 4), when the rhodamine-labeled sheets were excited at 543 nm, the entire sheet turned red with a measured emission wavelength of over 570 nm [Fig. 4(a)]. On the other hand, we tried to detect the NBD on the surface of the sheet as yellow at the excitation of 458 nm and at the emission wavelength region from 500 to 530 nm. We could observe that the obverse surface of the sheet was colored yellow, and the reverse side (bent site) was significantly quenched [Fig. 4(b)]. Since the FRET efficiency is related to the inverse six power of the distance between the acceptor and donor probes, the technique is elegantly used to measure the molecular distance at the 1.5–7.5 nm range.[34,35] Based on the earlier information and judging from the thickness of the rHSA-nanosheet, the quenching of the NBD emission from the bent side of the nanosheet was caused by the FRET effect from NBD to rhodamine. It also indicates that the NBD-latex beads are attached only to the obverse side of the nanosheet. If a sufficient amount of the NBD-latex beads were attached to both sides of the

sheet, then both sides of the sheet would be quenched. Furthermore, we also confirmed that the latex beads were specifically conjugated to the obverse side of the rHSA-nanosheets using an SEM [Fig. 4(e,f)]. The nanosheets released from the substrate after conjugating the latex beads were heterogeneously modified.

In the final step, we investigated a method to detach the rHSA-nanosheets from the patterned ODS-SAM. We selected $C_{12}E_{10}$ as a nonionic surfactant for which surfactant ability was independent of pH change. As shown in Table I, when the substrate, to which rHSA (non-SH modification) molecules were adsorbed, was immersed into a 1% (v/v) solution of $C_{12}E_{10}$ for 1 h at r.t., the water contact angle was returned to that of the ODS-SAM before rHSA adsorption. This indicated that the rHSA adsorbed on the ODS-SAM was detached by the addition of a $C_{12}E_{10}$, and the attractive force giving rise to the adsorption of rHSA on the ODS-SAM was hydrophobic interaction. In the first and second processes, the SH-rHSA molecules were selectively adsorbed onto the patterned ODS regions and crosslinked in the presence of copper ion (II) to prepare the rHSA-nanosheets. Very few of the resulting nanosheets were detached from the substrate by immersion in the 1% $C_{12}E_{10}$ solution for 1 h, whereas the control rHSA could simply detach. It took at least 6 h to detach the nanosheet from the substrate with the 1% $C_{12}E_{10}$ solution. On the other hand, we also conformed that the nanosheets were completely dissolved after 1 h by a DTT treatment (data not shown). This suggested that it was difficult for the $C_{12}E_{10}$ molecules to diffuse into the spaces between the nanosheets and the ODS-SAM substrate, because the nanosheet was composed of sufficiently two-dimensionally crosslinked rHSA by intermolecular oxidation of thiol groups. Furthermore, we confirmed that the resulting rHSA-nanosheets were stable in the presence of $C_{12}E_{10}$, because the sheet shapes did not change after the $C_{12}E_{10}$ removal by dialysis (data not shown).

Using a confocal laser scanning microscopy, we fortunately observed the rHSA-nanosheets in three-dimensional images and confirmed them to be a curved form [Fig. 2(c), and figure of supporting information]. On the basis of analyses of quartz crystal microbalance and grazing angle infrared spectroscopy, Roach et al. reported that albumin had enough adsorption affinity toward the hydrophobic (CH_3 terminus) compared to the hydrophilic surface (OH terminus), to cause adsorption-induced deformation.[36] Furthermore, Zeng et al. showed through modeling that the orientation of the adsorbed protein (lysozyme) was dependent on the discrete organization of the functional groups presented on the SAM surface, and in the case of the hydrophobic CH_3 group, hydrophobic amino residues of the protein were closest to the surface.[37] From these references, we suggested that the rHSA-nanosheets would adopt a curved form, because the wettability of the obverse and reverse surface of the rHSA-nanosheets was different, that is, the obverse surface appeared to be more hydrophilic than the reverse surface. Consequently, we succeeded in the detachment of the rHSA-nanosheets from the ODS-SAM by mild conditions such as surfactant immersion in order to obtain uniform rHSA-nanosheets.

CONCLUSIONS

We succeeded in the preparation of free-standing rectangular (10 × 30 μm) and ultrathin (4.5 ± 1.0 nm) rHSA-nanosheets by two-dimensional crosslinking via disulfide bonds on a patterned ODS-SAM, and could also obtain free-standing rHSA-nanosheets having heterosurfaces by surface modification with fluorescent latex beads. Thus, the rHSA-nanosheets may be a suitable candidate as a new biomaterial for drug-delivery carriers, hemostatic reagents, wound dressing for burn injury, and so forth. In our future work, we are preparing the rHSA-nanosheets on a large scale to carry the recombinant fragments of platelet membrane protein and/or dodecapeptides such as GPIbα and H12 to evaluate their performance *in vitro* and *in vivo*.

Y.O. was the recipient of a Research Fellowships from the JSPS for Young Scientists and the recipient of Japan Health Sciences Foundation.

References

1. Tomii Y. Lipid formation as a drug carrier for drug delivery. Cur Pharma Design 2002;8:467–474.
2. Takeoka S, Teramura Y, Okamura Y, Handa M, Ikeda Y, Tsuchida E. Fibrinogen-conjugated albumin polymers and their interaction with platelets under flow conditions. Biomacromolecules 2001;2:1192–1197.
3. Takeoka S, Teramura Y, Ohkawa H, Ikeda Y, Tsuchida E. Conjugation of von Willebrand factor-binding domain of platelet glycoprotein Ibα to size-controlled albumin microspheres. Biomacromolecules 2000;1:290–295.
4. Teramura Y, Okamura Y, Takeoka S, Tsuchiyama H, Narumi H, Kainoh M, Handa M, Ikeda Y, Tsuchida E. Hemostatic effects of polymerized albumin particles bearing rGPIa/IIa in thrombocytopenic mice. Biochem Biophys Res Commun 2003; 306:256–260.
5. Okamura Y, Takeoka S, Teramura Y, Maruyama Y, Tsuchida E, Handa M, Ikeda Y. Hemostatic effects of fibrinogen-γ chain dodecapeptide-conjugated polymerized albumin particles *in vitro* and *in vivo*. Transfusion 2005;45:1221–1228.
6. Takeoka S, Teramura Y, Okamura Y, Tsuchida E, Handa M, Ikeda Y. Rolling properties of rGPIbα-conjugated phospholipid vesicles with different membrane flexibilities on vWf surface under flow conditions. Biochem Biophys Res Commun 2002;296:765–770.

7. Okamura Y, Maekawa I, Teramura Y, Maruyama Y, Tsuchida E, Handa M, Ikeda Y, Takeoka S. Hemostatic effects of phospholipid vesicles carrying fibrinogen-γ chain dodecapeptide *in vitro* and *in vivo*. Bioconjug Chem 2005;16:1589–1596.
8. Okamura Y, Handa M, Suzuki H, Ikeda Y, Takeoka S. New strategy of platelet substitutes for enhancing platelet aggregation at high shear rates; cooperative effects of a mixed system of fibrinogen γ-chain dodecapeptide- or glycoprotein Ibα-conjugated latex beads under flow conditions. J Artif Organs 2006;9:251–258.
9. Takeoka S, Okamura Y, Teramura Y, Watanabe N, Suzuki H, Tsuchida E, Handa M, Ikeda Y. Function of fibrinogen γ-chain dodecapeptide-conjugated latex beads under flow. Biochem Biophys Res Commun 2003;312:773–779.
10. Mattson J, Forrest JA, Borjesson L. Quantifying glass transition behaviour in ultrathin free-standing polymer films. Phys Rev E 2000;62:5187–5200.
11. Tang Z, Kotov NA, Magonov S, Ozturk B. Nanostructured artificial nacre. Nat Mater 2003;2:413–418.
12. Mallwitz F, Laschewsky A. Direct access to stable, freestanding polymer membranes by layer-by-layer assembly of polyelectrolytes. Adv Mater 2005;17:1296–1299.
13. Mamedov A, Kotov NA, Prato M, Guldi DM, Wicksted JP, Hirsch A. Molecular design of strong single-wall carbon nanotube/polyelectrolyte multiplayer composites. Nature Mater 2002;1:190–194.
14. Huck WT, Stroock AD, Whitesides GM. Synthesis of geometrically well-defined, molecularly thin polymer films. Angew Chem Int Ed 2000;39:1058–1061.
15. Mamedov A, Kotov N. Free-standing layer-by-layer assembled films of magnetite nanoparticles. Langmuir 2000;16:5530–5533.
16. Mallwitz F, Goedel WA. Physically cross-linked ultrathin elastomeric membranes. Angew Chem Int Ed 2001;40:2645–2647.
17. Eck W, Küller A, Grunze M, Völkel B, Gölzhäuser A. Freestanding nanosheets from crosslinked biphenyl self-assembled monolayers. Adv Mater 2005;17:2583–2587.
18. Xu H, Goedel WA. Polymer-silica hybrid monolayers as precursors for ultrathin free-standing porous membranes. Langumuir 2002;18:2363–2367.
19. Nardin C, Winterhalter M, Meier W. Giant free-standing ABA triblock copolymer membranes. Langmuir 2000;16:7708–7712.
20. Ulman A. An Introduction to Ultrathin Organic Films from Langmuir–Blodgett to Self-Assembly. San Diego, CA: Academic Press; 1991.
21. Khoshtariya DE, Wei J, Liu H, Yue H, Waldeck DH. Charge-transfer mechanism for cytochrome c adsorbed on nanometer thick films. Distinguishing frictional control from conformational gating. J Am Chem Soc 2003;125:7704–7714.
22. Ferapontova EE, Shipovskov S, Gorton L. Bioelectrocatalytic detection of theophylline at theophylline oxidase electrodes. Biosens Bioelectron 2007;22:2508–2515.
23. Niwa D, Yamada Y, Homma T, Osaka T. Formation of molecular templates for fabricating on-chip biosensing devices. J Phys Chem B 2004;108:3240–3245.
24. Sugimura H, Ushiyama H, Hozumi A, Takai O. Micropatterning of alkyl- and fluoroalkylsilane self-assembled monolayers using vacuum ultraviolet light. Langmuir 2000;16:885–888.
25. Cavallini D, De Marco C, Dupre S, Rotilio G. The copper-catalyzed oxidation of cysteine to cystine. Arch Biochem Biophys 1969;130:354–361.
26. Wadu-Mestherige K, Amro NA, Liu GU. Immobilization of proteins on self-assembled monolayers. Scanning 2000;22:380–288.
27. Siqueira PDF, Wenz G, Schunk P, Schimmel T. An improved method for the assembly of amino-terminated monolayers on SiO_2 and the vapor deposition of gold layers. Langmuir 1999;15:4520–4523.
28. Depalma V, Tillman N. Friction and wear of self-assembled trichlorosilane monolayer films on silicon. Langmuir 1989;5:868–872.
29. Norde W, Giesbers M, Pingsheng H. Langmuir–Blodgett films of polymerized 10,12-pentacosadiyonic acid as substrates for protein adsorption. Colloids Surf B 1995;5:255–263.
30. Prime KL, Whitesides GM. Adsorption of proteins onto surfaces containing end-attached oligo(ethylene oxide): A model system using self-assembled monolayers. J Am Chem Soc 1993;115:10714–10721.
31. Komatsu T, Oguro Y, Teramura Y, Takeoka S, Okai J, Anraku M, Otagiri M, Tsuchida E. Physicochemical characterization of cross-linked human serum albumin dimer and its synthetic heme hybrid as an oxygen carrier. Biochim Biophys Acta 2004;1675:21–31.
32. Komatsu T, Oguro Y, Nakagawa A, Tsuchida E. Albumin clusters: Structurally defined protein tetramer and oxygen carrier including thirty-two iron(II) porphyrins. Biomacromolecules 2005;6:3397–3403.
33. Carter DC, Ho JX. Structure of serum albumin. Adv Protein Chem 1994;45:153–204.
34. Stryer L, Haugland RP. Energy transfer: A spectroscopic ruler. Proc Natl Acad Sci USA 1967;58:719–726.
35. Stryer L. Fluorescence energy transfer as a spectroscopic ruler. Ann Rev Biochem 1978;47:819–946.
36. Roach P, Farrar D, Perry CC. Interpretation of protein adsorption: Surface-induced conformational changes. J Am Chem Soc 2005;127:8168–8173.
37. Zeng J, Li L, Chen S, Jiang S. Molecular simulation study of water interactions with oligo (ethylene glycol)-terminated alkanethiol self-assembled monolayers. Langmuir 2004;20:8931–8938.

J Biorheol (2009) 23:29–34
DOI 10.1007/s12573-009-0005-0

ORIGINAL ARTICLE

Motion of polymerized albumin particles in a model arteriole in the presence of red blood cells

Tetsuya Tsuji · Shinji Takeoka · Yosuke Okamura · Ryo Sudo · Yasuo Ikeda · Kazuo Tanishita

Received: 9 January 2009 / Accepted: 9 April 2009 / Published online: 19 May 2009

Abstract Polymerized albumin particles (poly Alb) with recombinant glycoprotein Ibα (rGPIbα-poly Alb) are a promising candidate for a platelet substitute. Thus, we focused on the lateral motion of poly Alb in the presence of red blood cells, because the lateral motion plays an important role in aggregate formation. We visualized the microscopic motion of poly Alb toward the immobilized ligand (von Willebrand factor, VWF) surface in a model arteriole with red blood cells with a high-speed camera. At a higher shear rate of 1,500 s^{-1}, the concentration profile of poly Alb appeared to peak near the wall. This profile enhances the interaction between the particles and wall. Particularly the migration angle, being the angle of the poly Alb velocity vector, was enlarged near the wall and contributed to transfer of poly Alb toward the immobilized VWF surface. This tendency is desirable to achieve the adhesion of particles on the wall.

T. Tsuji · K. Tanishita (✉)
Department of System Design Engineering,
Keio University, 3-14-1 Hiyoshi, Kohoku-Ku,
Yokohama 223-8522, Japan
e-mail: tanishita@sd.keio.ac.jp

S. Takeoka · Y. Okamura
Department of Polymer Chemistry,
Waseda University, 3-4-1 Ohkubo, Shinjyuku-ku,
Tokyo 169-8555, Japan

R. Sudo
Department of Biological Engineering,
MIT, Cambridge, MA, USA

Y. Ikeda
School of Medicine, Keio University,
35 Shinanomachi, Shinjyuku-ku,
Tokyo 160-8582, Japan

Keywords Platelet substitute · Von Willebrand factor · Polymerized albumin particles · Lateral motion

Introduction

Platelet transfusion is the most effective therapy for bleeding associated with thrombocytopenia induced by chemotherapy or surgery, and the amount of platelets transfused each year has grown rapidly [1]. However, two important problems arise for platelet transfusion, namely the limitation of short-term storage and the risks of platelet transfusion, such as viral infections [2–4]. Therefore, it is difficult to supply enough platelets for such a large demand.

To overcome these problems, the development of platelet substitutes is necessary to facilitate long-term storage and avoidance of viral infections. In 1980, Coller [1] demonstrated that fibrinogen-coated beads interacted with platelets to perform the aggregation process. Agam and Livne [5] showed that platelet-bearing cross-linked fibrinogen aggregated with fresh platelets. Agam and Livne [6] also showed that erythrocytes with covalently bound fibrinogen participated in platelet aggregation and were effective for arresting bleeding in an animal model of autoimmune thrombocytopenia. Murata et al. [7] developed the prototype of platelet substitutes, rGPIbα-liposomes, which are produced by conjugating a recombinant glycoprotein (GP)Ibα (an adhesive receptor on a platelet) to the phospholipid surface of liposomes. Specific agglutination of the rGPIbα-liposomes to platelets was observed in the presence of von Willebrand factor (VWF) and ristocetin [8]. Recently, Takeoka et al. [9] developed polymerized albumin particles conjugated with recombinant glycoprotein Ibα (rGPIbα-poly Alb) and showed the shear-dependent adhesive process in an in vitro experiment.

An important aspect to anticipate the clinical feasibility is the microscopic motion of platelet substitutes in the blood flow, because the microscopic motion is directly involved in the formation of aggregates on the wall surface. Tangelder et al. [10] indicated that the concentration profile of platelets is in excess near the wall and that this enhanced the interaction between the platelets and vessel wall. Tilles et al. [11] recognized that the platelet-size beads formed such an excess near the wall in the presence of red blood cells (RBC). Furthermore, Goldsmith and Turitto [12] identified that the red blood cells directly augment the interaction with platelets or between the platelets and vessel wall.

In the present study, we employed rGPIbα-poly Alb (abbreviated by poly Alb) as a candidate for a platelet substitute. To verify the validity of poly Alb, we studied the fluid mechanical behavior of poly Alb in blood flow in the process of achieving hemostasis. Thus, we focused on the lateral motion of the poly Alb particles in a model arteriole in the presence of RBC, because the lateral motion will promote aggregate formation. The presence of RBC is essential to develop the peaked concentration of platelet substitutes near the wall. We visualized the microscopic motion of the particles toward the immobilized ligand (VWF)-coating surface in the rectangular duct flow chamber with a high-speed camera.

Materials and methods

Polymerized albumin particles

The polymerized albumin particles conjugated with recombinant glycoprotein (*r*GPIbα-poly Alb) were prepared according to the procedure developed by Takeoka et al. [9]. The particle diameters are 1,900 ± 400 nm. The particles were labeled with fluorescein isothiocyanate in which the excitation and emission wavelengths were 495 and 520 nm, respectively.

Flow chamber and VWF coating

To observe the motion of poly Alb approaching the wall, we built a rectangular duct consisting of two 0.2-mm-thick cover slips and two plates, as shown in Fig. 1. The

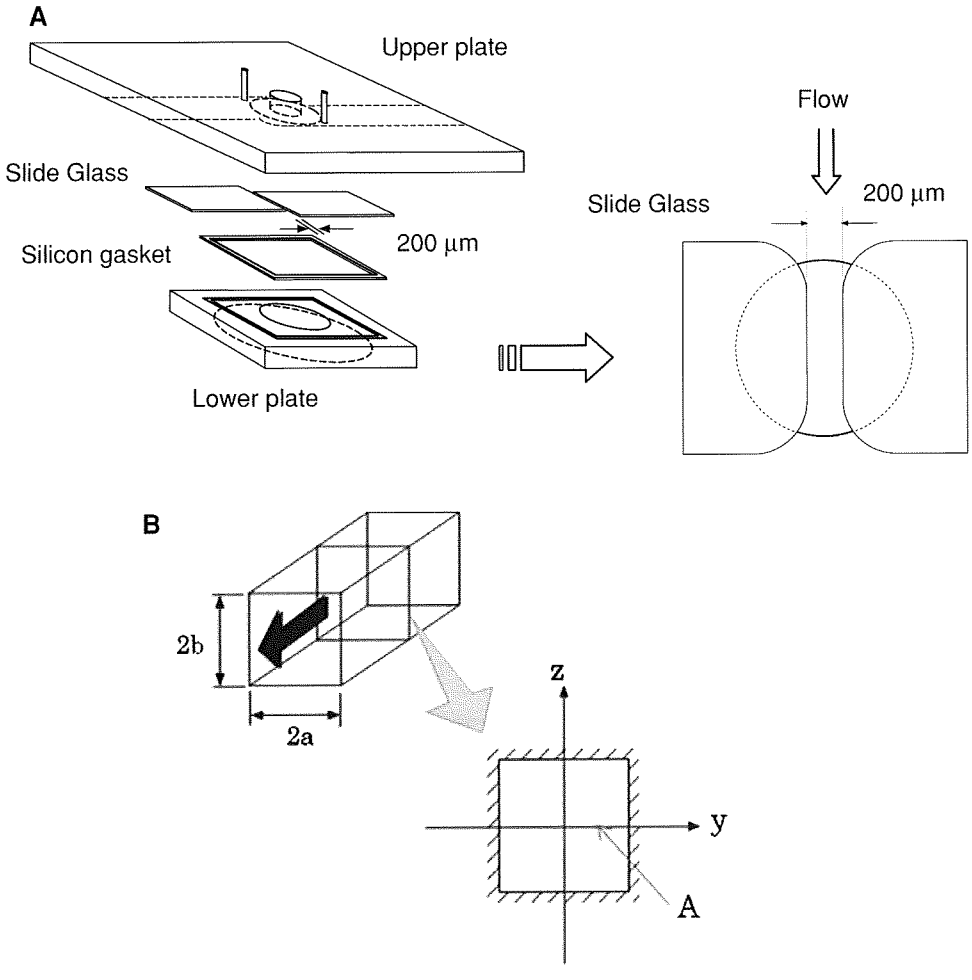

Fig. 1 Structure of rectangular flow chamber. **a** Overview of flow chamber. **b** The cross-section of the flow channel. Side A is the surface of the immobilized vWF

rectangular duct design was chosen as a model arteriole, which is an important region for hemostasis, because the velocity profile on the y-axis is very close to that in a circular pipe, and the image of poly Alb movement is not distorted in a rectangular duct. Thus, a rectangular duct with 0.2-mm sides was built. A side of the rectangular duct, designated by A in Fig. 1, was coated with von Willebrand factor (VWF) according to the procedure by Nishiya et al. [13].

Experimental system to visualize the particle motion

Figure 2 illustrates the experimental system to visualize the particle motion. A flow chamber was mounted on an inverted fluorescent microscope (Diaphoto, Nikon) and filled with phosphate buffer solution (pH 7.4 at 0°C) suspended with poly Alb and red cell ghosts. The concentration of poly Alb was 5 μg/ml. A steady gravity flow was introduced from the upper reservoir into the flow chamber. We measured the velocity distribution in the rectangular duct by tracer particle displacement and confirmed that the velocity profile agreed with the following theoretical prediction [14].

$$u = -\frac{1}{2\mu}\cdot\frac{dp}{dx}\left\{\left(b^2 - z^2\right) + \frac{32b^2}{\pi^3}\sum_{n=0}^{\infty}\frac{(-1)^{n+1}}{(2n+1)^3}\cdot \frac{\cosh\frac{(2n+1)\cdot\pi\cdot y}{2b}}{\cosh\frac{(2n+1)\cdot\pi\cdot a}{2b}}\cdot\cos\frac{(2n+1)\cdot\pi\cdot z}{2b}\right\} \quad (1)$$

where width of the cross-section is: 2a, height: 2b, and dp/dx: pressure gradient in x-direction.

We measured the velocity profile in the channel and determined the flow rate by integrating the velocity profile. The flow rates were 5.6×10^{-3} and 4.3×10^{-2} ml/min, corresponding to the Reynolds number 0.15 and 1.19, respectively. The corresponding wall shear rates are 190 and 1,500 s^{-1}, respectively.

We recorded the images of the poly Alb moving in the flow with a high-speed video camera (Speed Cam+, Weinverger AG, Switzerland). Since the duration time at high-speed recording was less than 1 ms, we used the Image Intensifier (XX1420AA, DHT, Japan) to amplify the weak fluorescence and also used an argon-ion laser (100 mW, ILT 5490ACM-01-5A, Ion Laser Technology) for strong excitation. With this high-speed and high-sensitivity experimental system, we could visualize the particle motion even at a shear rate of 1,500 s^{-1}, and then analyzed the concentration profiles and lateral motion of the particles.

Preparation of red cell ghosts suspension

Because the presence of red blood cells affects the motion of platelets significantly [9], we need to have a solution suspended with not only the poly Alb, but also red blood cells. Furthermore, we need to prepare the red cell ghosts to visualize the poly Alb particles in the flow. Goldsmith et al. [15] reported that the motion of red cell ghosts was very close to that of natural red blood cells, and Aparts et al. [16] in 1988 confirmed that the concentration profiles of platelets in the red cell ghost suspension were similar to that in the washed blood cell suspension.

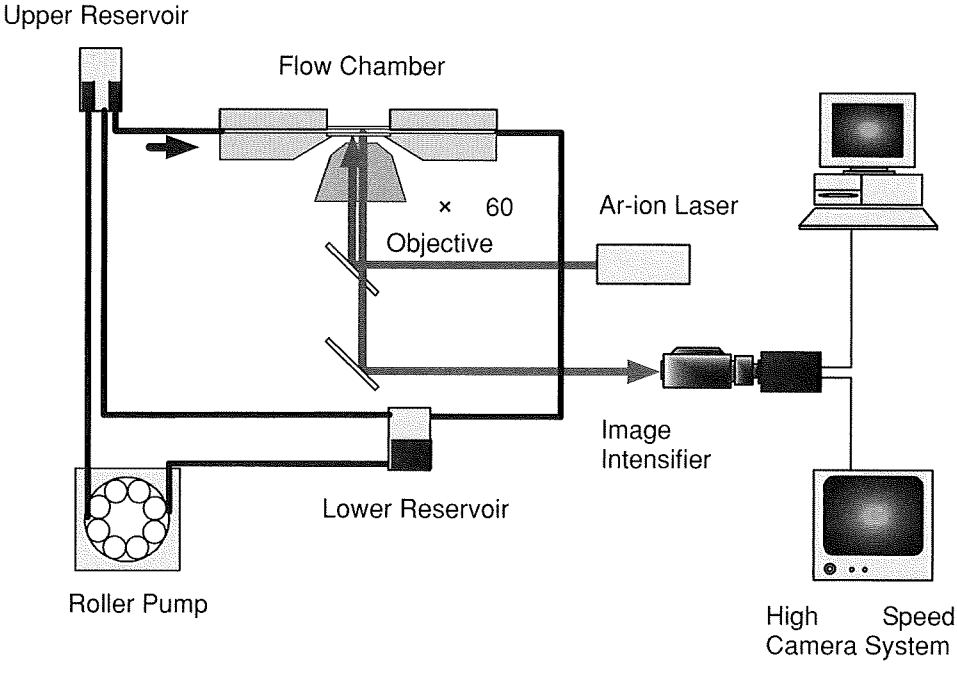

Fig. 2 Schematic diagram of the experimental circuit. The steady gravity flow is generated between the upper and lower reservoir, and the image of particle motion is taken by a high-speed camera system